# High-temperature behavior of oxide dispersion strengthening CoNiCrAlY

K.A. Unocic,[a] J. Bergholz,[b] T. Huang,[c,d] D. Naumenko,[c] B.A. Pint,[a] R. Vaßen,[b] W.J. Quadakkers[c]

[a]Materials Science and Technology Division, Oak Ridge National Laboratory, Oak Ridge, TN 37831, United States

[b]Institute for Energy and Climate Research, IEK-1 Forschungszentrum Jülich GmbH, 52425 Jülich, Germany

[c]Institute for Energy and Climate Research, IEK-2 Forschungszentrum Jülich GmbH, 52425 Jülich, Germany

[d]Kunming University of Science and Technology, Faculty of Materials Science and Engineering, 650093 Kunming, China

Key words: CoNiCrAlY coating, LPPS, oxidation, alumina scale, hafnium, yttrium, oxide dispersion strengthening

## Abstract

To investigate the effect of oxide dispersion strengthening (ODS) on bond coating performance, commercial Co-30wt.%Ni-20Cr-8Al-0.4Y powder was milled with 2% additions of $Al_2O_3$, $Y_2O_3$ or $Y_2O_3$+$HfO_2$. Free-standing specimens were made by low-pressure plasma spraying (LPPS) and oxidized at 1100°C both isothermally (100 h) in air+10%$H_2O$ and using 1-h cycles in air±10%$H_2O$ for 500 cycles. Dry air cyclic testing was conducted at both ORNL and FZJ with remarkably similar results. Two LPPS specimens without oxide additions were tested for comparison. The specimens with 2%$Al_2O_3$ addition exhibited the best behavior as the powder already contained 0.4%Y. Additions of 2%$Y_2O_3$ and especially 1%$Y_2O_3$+1%$HfO_2$ resulted in over-doping as evidenced by high mass gains and the formation of Y- and Hf-rich pegs. In general,

water vapor caused typical effects of more scale spallation. The isothermal specimens were characterized using analytical scanning transmission electron microscopy (STEM). In the over-doped specimens, Hf and/or Y segregation to the alumina scale grain boundaries was not observed.

## Introduction

In searching for improved bond coatings for thermal barrier coating (TBC) systems for land-based gas turbines, a recent observation was that an air plasma sprayed (APS) "flash" coating on top of a high velocity oxygen fuel (HVOF) MCrAlY coating resulted in a substantial improvement in furnace cycle lifetime [1,2]. One explanation for this improvement is an increased roughness compared to typical HVOF coatings that provides better bonding with the APS yttria-stabilized zirconia (YSZ) top coating. However, the outer APS bond coating layer also contains a higher content of oxide particles. It is well-known that oxide dispersion strengthening (ODS) can lead to improvements in oxidation behavior and, in particular, effects associated with a higher creep strength substrate [3-7].

To study the potential ODS benefit on the oxidation performance of MCrAlY bond coatings, this study fabricated free-standing ODS CoNiCrAlY specimens using LPPS and characterized the reaction products after both isothermal and cyclic oxidation testing at 1100°C. Cyclic oxidation testing using 1-h cycles was conducted at both Oak Ridge National Laboratory (ORNL) and at Forschungszentrum Jülich (FZJ). Characterization of the reaction products was used to better understand the oxidation results including how the reactive element (RE) addition might be optimized in the

coating, which also is dependent on the coating process [8]. The ODS as well as the non-ODS LPPS NiCoCrAlYHf and CoNiCrAlY specimens were used to illustrate these issues. Evaluations also included testing in air with 10%$H_2O$ environments to better simulate turbine exhaust and the detrimental effects of water vapor on bond coating oxidation behavior [9-13]

**Experimental Procedure**

Commercial Co-30wt.%Ni-20Cr-8Al-0.4Y powder (Amdry 9954, -90+45 µm; purchased from Erlikon Metco, Wohlen, Schweiz) was ball milled with 2 wt.% additions of either (1) $Al_2O_3$, (2) $Y_2O_3$, or (3) $Y_2O_3$+$HfO_2$. Additional details of the process development are detailed elsewhere [14]. The oxide dispersion powders were within -18+0.2 µm size range and were purchased from Martinswerk, Bergheim, Germany. Each batch was ball milled for 6 h in a static Ar atmosphere using a Simoloyer model CM01 ball mill (Zoz GmbH, Wenden, Germany). Stearic acid (Ligacid 10-12, $C_{18}H_{36}O_2$, Peter Greven GmbH & Co. KG, Bad Mustereifel, Germany) was used as a process control agent (PCA) to limit particle growth and ensure successful incorporation of the oxide particles [14]. After ball milling, the powders were sprayed via low pressure plasma spray (LPPS) on a steel plate including CoNiCrAlY and a NiCoCrAlYHf powder without an oxide addition, Table 1.

Oxidation coupons (10 x 20 x 1.5 mm) were cut from the steel plate using spark-erosion. The free-standing material was then heat-treated in vacuum of $10^{-5}$ mbar at 1120°C for 2 h followed by 24 h heat treatment at 845°C. The FZJ coupons were polished to a P1200 grit (15.3 µm) surface finish and ultrasonically degreased in ethanol.

The coupons at ORNL were polished to a 600 grit (16 μm) surface finish and ultrasonically cleaned in acetone and methanol prior to oxidation testing. Mass change was measured using a Mettler-Toledo model XP205 balance with an accuracy of 0.04 mg (or ±0.01 mg/cm$^2$). Specimens were tested at 1100°C (1) isothermally for 100 h using a Cahn model 1000 microbalance to measure the reaction kinetics using air with 10±1%$H_2O$ with a gas flow rate of 100 cc/min and (2) cyclically using 1-h cycles with 10 min cooling between cycles using an automated system with dry or wet (10% $H_2O$) air with a gas flow rate of 185 cc/min for 500 cycles. The specimens were weighed every 20 (ORNL) or 50 (FZJ) cycles.

After exposure, specimens were Cu- or Ni-plated and characterized in cross-section using light microscopy, scanning electron microscopy (SEM) (Hitachi model S4800) equipped with x-ray energy dispersive spectroscopy (EDS) (EDAX system) and a FEI Talos F200X operated at 200 kV, which is equipped with an extreme field emission gun (X-FEG) electron source and Super-X EDS (energy dispersive spectroscopy) system with 4 silicon drift detectors (SDD) for chemical analysis. Specimens for TEM analysis were prepared by focused ion beam (Hitachi model NB5000 FIB-SEM,) using the *in-situ* lift-out method from oxidized surfaces of only isothermally tested coupons. Electron backscatter diffraction (EBSD) analyses were acquired using a Zeiss Merlin SEM equipped with a Nordlys EBSD camera and Aztec software package (Oxford Instruments). Transmission Kikuchi diffraction (TKD) was performed on the scales using FEI Versa 3D Dual beam equipped with Aztec software package (Oxford Instruments). The β-phase depletion was measured from the gas/oxide interface because often the metal/oxide interface was difficult to be determined using the Fiji software.

## Results

*Cyclic oxidation*

Figure 1 shows the specimen mass change data for 1-h cycles at 1100°C. Figure 1a shows the data from ORNL and FZJ in dry air where remarkably similar results were observed in both laboratories. The non-ODS NiCoCrAlYHfSi specimens had the highest mass gain due to significant internal oxidation, Figure 2a. A non-ODS CoNiCrAlY specimen was only exposed at FZJ and showed significantly lower mass gain, Figure 1a. The ODS-CoNiCrAlY specimens with a 2%$Al_2O_3$ addition showed the lowest mass gain and formed a uniform, thin alumina scale, Figure 2b. The addition of 2%$Y_2O_3$ resulted in a slightly higher mass gain, similar to the non-ODS CoNiCrAlY specimen for ~250 cycles. The $Y_2O_3$-dispersed specimens then showed decreasing mass suggesting scale spallation. Consistent with the mass gain data, the oxide was thicker on this specimen, Figure 2c and the inset in Figure 2c shows an area where the scale spalled. Finally, the specimens with 1%$Y_2O_3$ and 1%$HfO_2$ showed a higher mass gain followed by evidence of scale spallation. In this case, there was some difference in spallation behavior between the ORNL and FZJ specimens, Figure 1a. The combination of $Y_2O_3$ and $HfO_2$ resulted in increased internal oxidation, Figure 2d, consistent with the higher initial mass gain.

Figure 3 shows the scale formed on the non-ODS CoNiCrAlY specimen. Consistent with the low mass gain in Figure 1a, a thin, fairly uniform scale was observed with only minor internal oxidation of the Y in the powder, Table 1. The SEM EDS maps in Figure 3 reveal that significant Y was incorporated into the scale during this exposure and the typical β depletion zone developed.

Figure 1b shows the effect of adding 10% water vapor on the cyclic oxidation behavior for cyclic tests conducted at ORNL. In general, the ODS specimens showed increased spallation with the addition of $H_2O$, while the non-ODS NiCoCrAlYHfSi specimen exposed in wet air showed a slightly higher mass gain. Cross-sections of the specimens cycled in wet air are shown in Figures 2e-2h and compared to the specimens exposed in dry air at ORNL. In both environments, the non-ODS NiCoCrAlYHfSi specimens formed a thick scale with significant internal oxidation. The bright particles in the BSE images are oxides rich in high atomic number elements Hf or Y. For the ODS specimens, the scales were thinner after exposure in wet air consistent with scale spallation. No internal oxidation was observed for the $Al_2O_3$-dispersed specimens. For the specimens with $Y_2O_3$ additions, Y-rich oxides in the scale were only clearly observed after oxidation in dry air, likely due to more scale spallation in wet air. In both environments, the specimens with both $Y_2O_3$ and $HfO_2$ additions showed significant internal oxidation with evidence of RE-rich oxide formation, particularly in the areas with the thickest scale, Figures 2d and 2h. These specimens also showed bright precipitates in the metal, which were identified as HfC. For the specimen exposed in wet air, there appeared to be a region depleted in HfC beneath the scale, Figure 2h.

Figure 4a quantifies the scale thicknesses shown in Figure 2 using box and whisker plots that show the 25% and 75% values along with the median value within the box. The whiskers show the minimum and maximum values measured. Consistent with the mass change data in Figure 1, the thinnest oxides were observed on the $Al_2O_3$-dispersed specimens followed by the $Y_2O_3$-dispersed specimens. However, for the exposures in water vapor, the scales may be thinner due to scale spallation. The thickest

oxides were observed on the non-ODS specimens and the measurements suggest that the addition of water vapor slightly increased the scale thickness, perhaps by increasing the degree of internal oxidation. As a measure of the amount of degradation, Figure 4b shows the depth of β-phase depletion in each of the specimens in Figure 2. Consistent with the mass change data in Figure 1b, water vapor had little effect on the depletion observed in the non-ODS NiCoCrAlYHfSi specimen. For the ODS CoNiCrAlY specimens, the β-phase depletion increased when the specimens were tested in water vapor, consistent with the increase in spallation. The largest depletion was observed for the specimens with 1%$Y_2O_3$ and 1%$HfO_2$, which is not surprising given the thicker scale that formed on these alloys. The significant increase in depletion for the $Al_2O_3$-dispersed specimen exposed to wet air seems unusual given the relatively small mass loss. In general, the CoNiCrAlY powder had a lower Al content and the depth of β phase depletion should not be compared with that of the NiCoCrAlYHfSi specimen.

The alloy microstructure also was examined ~200 μm below the surface after the 500 h cyclic exposure, Figure 5. As expected, the alloy grain size was smaller in the ODS specimens. The $Al_2O_3$-dispersed specimen appeared to have the finest grain size. In addition to the oxide particles inhibiting grain growth, the PCA addition appeared to further refine the microstructure [14]. Carbon residue from the PCA may have contributed to the formation of Cr-rich carbides. Note the very high C contents in the ODS specimens, Table 1. Figure 6 shows the SEM EDS Cr maps showing the Cr-rich precipitates in the ODS specimens, but they were typically not observed in the β depletion zone. For example, no Cr-rich precipitates were observed in Figure 6h because of the large depletion zone in the 1%$Y_2O_3$+1%$HfO_2$ ODS specimen after being cycled in

wet air. In contrast, many Cr-rich precipitates were observed in the $Al_2O_3$-dispersed specimen after cycling in dry air (Figure 6b) where the β depletion zone was small, Figure 4b. Also, no Cr-rich precipitates were observed in either NiCoCrAlYHfSi specimen, Figures 6a and 6e.

In both Hf containing specimens, HfC precipitates were observed and they appeared to contribute to grain size refinement. The high Z, Hf-rich precipitates appear bright in the SEM BSE images in Figure 7. In the NiCoCrAlYHfSi specimen, the grains were finer near the HfC precipitates, which were not uniformly dispersed. In the ODS specimen with $1\%Y_2O_3+1\%HfO_2$, there appears to be a larger fraction of HfC (consistent with the higher Hf content, Table 1) and a smaller grain size. A further examination of the air-cycled FZJ specimen with $1\%Y_2O_3+1\%HfO_2$ showed that HfC was present in the substrate at the edge of the β depletion zone, Figure 8a. Deeper in the substrate, Figure 8b, both HfC and Cr-rich $M_{23}C_6$ were present as suggested by the EDS Cr map in Figure 6d.

*Isothermal oxidation*

Because of the scale spallation observed in the cyclic testing, the only suitable way to carefully study the scale microstructure formed on the ODS specimens was in isothermal exposures at 1100°C. Exposures of 100 h were selected as this has been used in other studies of alumina-forming alloys [15-17]. Figure 9 shows the mass gain curves for each of the specimens in wet air. Similar to the cyclic oxidation results, the lowest mass gain was observed for the ODS specimen with $2\%Al_2O_3$ and the highest mass gains were for the ODS and non-ODS specimens containing Hf (parabolic rate constants of $3x10^{-12}$ and $1x10^{-11}$ $g^2/cm^4s$, respectively). The rate for the ODS specimen with $2\%Al_2O_3$ was $3x10^{-}$

$^{13}$ $g^2/cm^4s$, which was very similar to the non-ODS CoNiCrAlY specimen ($6x10^{-13}$ $g^2/cm^4s$). The rate for the ODS specimen with 2%$Y_2O_3$ was $1x10^{-12}$ $g^2/cm^4s$.

Cross-sections of the oxide scales after 100 h are shown in Figure 10. (Unfortunately, the non-ODS CoNiCrAlY specimen was obtained later and was not included in the characterization.) Similar to the scales formed in cyclic testing and consistent with the mass change data, thicker scales formed on the Hf-containing alloys (ODS and non-ODS) and a very thin uniform scale formed on the $Al_2O_3$-dispersed CoNiCrAlY specimen.

Figure 11 summarizes the STEM observations for the four specimens in Figure 10 showing both bright field (BF) and high angle annular dark field (HAADF) images of each specimen. The thicker, less uniform scales on the Hf-containing alloys were more difficult to section and get a representative area for characterization than the more uniform scales formed on the ODS specimens with 2%$Al_2O_3$ (Figures 11b and 11f) and 2%$Y_2O_3$ (Figures 11c and 11g). In general, the scales formed columnar scales with an outer layer of more equiaxed grains. Figure 12 shows higher magnification STEM HAADF images of the outer layer on each of the specimens. Voids and RE-rich precipitates were frequently observed in this layer while the inner columnar layer tended to be denser. Both the inner and outer scales were identified as $\alpha$-$Al_2O_3$. As an example, Figure 13 shows electron diffraction analysis of the inner and outer scale layers formed on the NiCoCrAlYHfSi specimen. Both electron diffraction patterns were oriented with the electron beam in the $[2\bar{1}\bar{1}0]$ direction. Analysis of the interplanar spacings and angles confirmed the presence of $\alpha$-$Al_2O_3$.

Figure 14 shows STEM HAADF images and EDS maps of the same four specimens. The maps confirm that where thicker scales formed, RE-rich oxide particles were incorporated into the scale, i.e. peg formation with the RE-rich oxide surrounded by alumina due to the fast O transport in RE oxides and/or at precipitate-alumina interfaces [18,19].

At a higher magnification, Figure 15 shows images of the slow-growing, mainly columnar scale formed on $Al_2O_3$-dispersed CoNiCrAlY. With the advanced EDS detection on the Talos STEM, grain boundary segregation of Y on most of the alumina scale grain boundaries can be found in one map. In addition, small Y-rich oxides were observed near the interface between the outer and inner oxide layers (Figure 12c) and in the substrate adjacent to the scale, Figure 15c. Recall that this Y was present in the starting CoNiCrAlY powder. The Cr EDS map in Figure 15d also shows some Cr incorporation in the outer scale. Surprisingly, in the other specimens with higher Hf and/or Y levels no grain boundary segregation of Y or Hf was detected (including attempts at higher magnification). In these specimens, the large RE additions appeared to be only found in the RE-rich oxides rather than segregated to the alumina grain boundaries.

Finally, the grain structure of the scales formed on the ODS specimens was analyzed using TKD, Figure 16. In general, the scale was less columnar on the Hf-containing specimen. The TKD showed similar orientations of the alumina grains even though there was a variation in the scale morphology. However, TKD showed more random grains in the outer equiaxed region. The phase maps also confirmed that the outer scales were $\alpha$-$Al_2O_3$, consistent with the electron diffraction analysis shown in

Figure 13. Figures 16a and 16c have more non-indexed pixels because of an issue with specimen preparation.

**Discussion**

While the initial goal was to study the role of an oxide dispersion on the oxidation behavior of free-standing bond coating compositions, in many cases the specimens were illustrations of RE over-doping, which has been discussed in a number of RE studies [8,21,22]. Overdoping was an issue because the starting powder contained Y and adding $HfO_2$ and/or $Y_2O_3$ then provided much more RE than necessary for optimal behavior. Table 1 clearly shows the lower Hf and Y values in the commercial powders compared to the ODS materials. The clearest evidence of the non-optimal behavior was the excessive formation of RE-rich oxide precipitates which permits rapid O transport through the alumina, resulting in much thicker scales. The overdoped scales also had a less columnar grain structure. Surprisingly, the overdoped scales also did not show segregation of Hf and/or Y ions to the alumina grain boundaries. A possible explanation is that nearby RE-rich oxides provide "sinks" for the RE ions, thus reducing the amount of segregation. Previously it was demonstrated that the amount of segregation dropped when RE-rich oxides precipitated [24]. The lack of RE segregants may explain the larger grains in the overdoped scales. In prior studies with over-doping, the thick scales were typically not studied by STEM, thus the lack of RE segregation in over-doped scales has not been previously reported.

The only ODS specimen that was not overdoped was the $Al_2O_3$-dispersed CoNiCrAlY, Figures 1 and 9. This composition showed the slowest scale growth rate

and best scale adhesion. However, the specimen cycled with water vapor in the environment did show noticeable scale spallation, Figure 1b and 2f. Smialek has suggested that this is due to a process similar to stress corrosion cracking at the metal-scale interface [11]. While stronger substrates do resist deformation [3,25], they also are unable to relax the thermal mismatch stress [26] and their oxide scales tend to spall more readily than those that form on weaker (e.g. non-ODS) substrates. Another reason for increased scale spallation from the ODS materials could be the high C content in the ODS materials. Cr-carbide formation at the metal-scale interface was shown to promote scale spallation during cyclic oxidation of model C-containing FeCrAlY alloys [27]. Indications of Cr-rich carbide formation at the scale/metal interface of the ODS-coatings studied in the present work can be found in Figure 6. Further studies are required to determine to what degree these two factors contributed to the observed scale spallation.

The non-ODS NiCoCrAlYHfSi specimens were not the optimal comparison for the ODS CoNiCrAlY specimens. Later in the project, non-ODS CoNiCrAlY was compared in the cyclic oxidation test in dry air, Figure 1a, and in the isothermal experiment, Figure 9. With less Y and no Hf, the mass gain was much lower than the NiCoCrAlYHfSi specimen and similar to the mass gains for the $Al_2O_3$- and $Y_2O_3$-dispersed specimens.

The non-ODS NiCoCrAlYHfSi specimens illustrated an important issue about the effect of coating O content on the optimal RE addition. This composition with ~0.25%Hf and 0.68%Y [22] may provide excellent results for cathodic arc and HVOF coatings [17,23] but the LPPS process used here typically results in a much lower O content that has been shown to produce non-optimal results for a fixed RE content in the powder [8].

When the coating contains a higher O level, the RE additions are tied up as oxides. Compared to RE alloy additions, the RE is less mobile when present as oxides and less RE becomes incorporated into the alumina scale [8,16,19], typically resulting in better oxidation performance. To produce optimal results, the Y and Hf levels should have been reduced in the powder for the LPPS process, although, it should be mentioned that overdoping also is a function of specimen/coating thickness [28,29].

The effect of water vapor observed in Figure 1b is typical of prior work [9-13]. Alumina is less affected by water vapor than chromia or silica scales [30,31], however, alumina-forming alloys and coatings can still show effects such as increased scale spallation and shorter TBC lifetimes [12,13,32]. The CoNiCrAlY with $Y_2O_3$ and $HfO_2$ appeared to show an initial faster scale growth rate in wet air compared to dry air. The other ODS specimens showed similar initial mass gains in both environments followed by increased spallation in the presence of water vapor. The isothermal testing was conducted with water vapor as this environment is more representative of the turbine operating conditions.

Several unique microstructural observations were noted. The formation of Cr-rich $M_{23}C_6$ can be attributed to the higher C content in the ODS material compared to the original powder, Table 1. In general, ball milling can lead to increased interstitials such as C, N and O during milling and handling of the powder. In this case, the PCA addition also likely further increased the C content. The apparent depletion of $M_{23}C_6$ in the β depletion zone, has been modeled previously for the case of alloy 602CA [33,34]. The depletion of $M_{23}C_6$ may be related to the effect of Al content on Cr activity, i.e. the decreased Al content in the subscale depletion zone results in a decreased Cr activity,

apparently resulting in a dissolution of the carbide phase. In addition to $M_{23}C_6$, HfC was observed in both Hf-containing materials. For the ODS material, this observation implies that the $HfO_2$ dispersion added during manufacturing dissociated and reacted with C introduced into the coating by the PCA. All of the ODS materials contain very high C levels, Table 1. A more complete thermodynamic assessment is needed. The HfC depletion observed in Figure 2h could be attributed to dissolution of the HfC as Hf becomes incorporated into the scale. This means that effectively a reverse transformation of Hf-carbide into Hf-oxide occurs. Again, these issues could be studied computationally considering the locally prevailing thermodynamic activities of Hf, C and O and diffusion controlled reactions.

The outer scale layer formed on the ODS CoNiCrAlY materials shown in Figure 11 contained RE-rich oxides, voids and enrichment of Cr from the transient phase of oxidation, Figure 15e. The observation of voids in this layer could be due to the $\alpha$–$\theta$ phase transformation [15,16,35], the solid state formation of $NiAl_2O_4$ [36] or the evaporation of Cr and/or Ni [37].

Similar powders with 2%$Y_2O_3$ and 1%$Y_2O_3$+1%$HfO_2$ were sprayed as bond coatings using HVOF with an APS YSZ top coating and compared to a conventional HVOF NiCoCrAlYHfSi bond coating [38]. In 100-h furnace cycle testing at 1100°C in wet air, all of these bond coatings showed a similar lifetime of 4 cycles. Thus, the ODS additions did not improve the TBC lifetime. However, based on this study, the $Al_2O_3$-dispersed powder also should have been evaluated. Subsequently, a >4X increase in TBC lifetime was observed when the APS flash coating was added to the conventional HVOF bond coating [2]. To further study the benefit of ODS bond coatings, future work

should focus on $Al_2O_3$-dispersed coatings with no further RE additions and lower C contents. In addition, quantifying the ODS effect on coating mechanical properties would be useful for modeling as well as studying how the volume fraction of oxide affects oxidation behavior. For actual coating studies, the ODS layer could be used as the flash coat layer with an HVOF inner layer.

**Conclusions**

Free standing bond coating compositions with and without oxide dispersion strengthening (ODS) were sprayed using low pressure plasma spray and evaluated in cyclic and isothermal oxidation at 1100°C. Detailed characterization of the scale and alloy microstructures were conducted in order to study the effect of different oxide dispersions on oxidation behavior in both dry air and air with 10%$H_2O$ to simulate turbine exhaust. For 1-h cyclic testing in dry air, similar results were obtained at FZJ and ORNL. Non-ODS NiCoCrAlYHfSi specimens experienced significant internal oxidation of Hf and Y resulting in high mass gains and thick scales in both 500, 1-h cycles and 100-h isothermal exposures. Likewise, CoNiCrAlY with additions of 2%$Y_2O_3$ and 1%$Y_2O_3$ + 1%$HfO_2$ showed faster scale growth, particularly for the latter composition. All three of these compositions were overdoped with Hf and/or Y. The best performing composition was with a 2%$Al_2O_3$ addition, which showed the lowest mass gains, best scale adhesion and limited β phase depletion beneath the scale. This was the only specimen where Y ions were found to strongly segregate to the alumina scale grain boundaries. All of the ODS specimens had a finer grain size. Similar to previous studies, the addition of water vapor in the cyclic testing resulted in increased oxide scale spallation for all of the ODS

compositions. The use of PCA to prepare the powder resulted in high levels of C in the specimens leading to the formation of Cr-rich $M_{23}C_6$ in all cases and HfC in the Hf-containing specimens. Future work should focus on $Al_2O_3$ dispersions to avoid issues with overdoping.

**Acknowledgments**

This work is part of a FZJ-ORNL collaboration where work in Germany was funded by the Federal Ministry of Education and Research (BMBF) through the project "High-Temperature and Energy Materials" under grant 03EK3032, and the stay of T. Huang was sponsored by the National Natural Science Foundation of China (Grant No. 51401097) and the China Scholarship Council. The U.S. work was funded by the U.S. Department of Energy, Office of Fossil Energy, Turbine Program. The microscopy at ORNL was supported (1) through a user proposal at ORNL's Center for Nanophase Materials Sciences (CNMS), which is a U.S. Department of Energy, Office of Science User Facility, and (2) by the U.S. Department of Energy, Office of Nuclear Energy, Fuel Cycle R&D Program and the Nuclear Science User Facilities. At ORNL, D.W. Coffey, T.M. Lowe, G.W. Garner, T. Jordan, T.S. Geer, assisted with the experimental work. S. Dryepondt and J. A. Haynes provided comments on the manuscript. At FZJ, the authors are grateful to their colleagues for spraying the coatings (K.-H. Rauwald, R. Laufs), carrying out the oxidation experiments (A. Kick, H. Cosler) and conducting SEM and EBSD analyses (Dr. E. Wessel and Dr. D. Grüner).

## References


1. W. Nowak, D. Naumenko, G. Mor, F. Mor, D. E. Mack, R. Vassen, L. Singheiser and W.J. Quadakkers, “Effect of processing parameters on MCrAlY bondcoat roughness and lifetime of APS–TBC systems,” Surf. Coat. Technol. 260 (2014) 82–89.
2. B. A. Pint, M. J. Lance and J. A. Haynes, (2017) “The Effect of Coating Composition and Geometry on TBC Lifetime,” ASME Paper #GT2017-65103, for the International Gas Turbine & Aeroengine Congress & Exhibition, Charlotte, NC, June 26-30, 2017.
3. H. E. Evans, "Stress Effects in High Temperature Oxidation of Metals," *International Materials Review* **40**, 1-40 (1995).
4. M. Schütze, "An Approach to a Global Model of the Mechanical Behavior of Oxide Scales," *Materials at High Temperature* **12**, 237-47 (1994).
5. W. J. Brindley, J. D. Whittenberger, "Stress Relaxation of Low Pressure Plasma-Sprayed NiCrAlY Alloys" Mat. Sci. and Eng. A163 (1993) 33-41.
6. A. G. Evans, D. R. Mumm, J. W. Hutchinson, G. H. Meier and F. S. Pettit, "Mechanisms Controlling the Durability of Thermal Barrier Coatings," Progress in Materials Science, 46 (2001) 505-53.
7. B. A. Pint, A. J. Garratt-Reed and L. W. Hobbs, "The Reactive Element Effect in Commercial ODS FeCrAl Alloys," *Materials at High Temperature* **13**, 3-16 (1995).
8. D. Naumenko, B. A. Pint and W. J. Quadakkers, “Current thoughts on reactive element effects in alumina-forming systems - in memory of John Stringer,” Oxidation of Metals, 86 (2016) 1-43.
9. C. Leyens, K. Fritscher, R. Gehrling, M. Peters and W. A. Kaysser, “Oxide Scale Formation on an MCrAlY Coating in Various $H_2$-$H_2O$ Atmospheres,” Surf. Coat. Tech., 82 (1996) 133-144.
10. R. Janakiraman, G. H. Meier and F. S. Pettit, “The Effect of Water Vapor on the Oxidation of Alloys that Developed Alumina Scales for Protection,” Met. Mater. Trans., 30A (1999) 2905-2913.
11. J. L. Smialek, “Enigmatic Moisture Effects on $Al_2O_3$ Scale and TBC Adhesion,” Mater. Sci. Forum, 595-598 (2008) 191-198.
12. V. Déneux, Y. Cadoret, S. Hervier, and D. Monceau, “Effect of Water Vapor on the Spallation of Thermal Barrier Coating Systems During Laboratory Cyclic Oxidation Testing,” Oxid. Met. 73 (2010) 83-93.
13. B. A. Pint, K. A. Unocic and J. A. Haynes, “The Effect of Environment on TBC Lifetime,” J. Eng. Gas Turb. & Power, 138 (8) (2016) 082102.
14. J. Bergholz, B. A. Pint, K. A Unocic and R. Vaßen, “Fabrication of Oxide Dispersion Strengthened Bond Coats with Low $Al_2O_3$ Content,” J. Therm. Spray Tech. 26 (2017) 868-879.
15. B. A. Pint, K. L. More, I. G. Wright and P. F. Tortorelli, "Characterization of Thermally Cycled Alumina Scales," *Materials at High Temperature*, 17, (2000) 165-71.
16. B. A. Pint and K. L. More, “Characterization of Alumina Interfaces in TBC Systems,” J. Mater. Sci. 44 (2009) 1676-86.

17. K. A. Unocic and B. A. Pint, “Characterization of the Alumina Scale Formed on a Commercial MCrAlYHfSi Coating,” Surface and Coatings Technology, 205 (2010) 1178-1182.
18. H. Hindam and D. P. Whittle, "Peg Formation by Short-Circuit Diffusion in $Al_2O_3$ Scales Containing Oxide Dispersions," J. Electrochem. Soc., 129 (1982) 1147-1149.
19. E. Hejrani, D. Sebold, W.J. Nowak, G. Mauer, D. Naumenko, R. Vassen, W. J. Quadakkers, “Isothermal and cyclic oxidation behavior of free standing MCrAlY coatings manufactured by high-velocity atmospheric plasma spraying,” Surface & Coatings Technology 313 (2017) 191–201.
20. B. A. Pint and K. B. Alexander, "Grain Boundary Segregation of Cation Dopants in $\alpha$-$Al_2O_3$ Scales," *Journal of the Electrochemical Society*, **145** (1998) 1819-29.
21. B. A. Pint, "Optimization of Reactive Element Additions to Improve Oxidation Performance of Alumina-Forming Alloys," *Journal of the American Ceramic Society*, **86** (2003) 686-695.
22. J. T. DeMasi-Marcin and D. K. Gupta, “Protective coatings in the gas turbine engine,” Surface and Coatings Technology, 68-69 (1994) 1–9.
23. J. A. Haynes, K. A. Unocic and B. A. Pint, “Effect of Water Vapor on the 1100°C Oxidation Behavior of Plasma-Sprayed TBCs with HVOF NiCoCrAlX Bond Coats,” Surface and Coatings Technology, 215 (2013) 39-45.
24. B. A. Pint, A. J. Garratt-Reed and L. W. Hobbs, "Possible Role of the Oxygen Potential Gradient in Enhancing the Diffusion of Foreign Ions on □-Al2O3 Grain Boundaries," *Journal of the American Ceramic Society* **81**, 305-14 (1998).
25. S. Dryepondt and B. A. Pint, “Effect of Substrate Mechanical Properties on Alumina Scale Morphology,” *Materials Science and Engineering* 497 (2008) 224-230.
26. H. Echsler, E. Alija Martinez, L. Singheiser and W. J. Quadakkers, “Residual Stresses in Alumina Scales Grown on Different Types of Fe-Cr-Al Alloys: Effect of Specimen Geometry and Cooling Rate,” Mater. Sci. Eng., A384 (2004) 1-11.
27. V. Kochubey, D. Naumenko, E. Wessel, J. Le Coze, L. Singheiser, H. Al-Badairy, G. J. Tatlock and W. J. Quadakkers, “Evidence of Cr-Carbide Formation at the Scale/Metal Interface During Oxidation of FeCrAl Alloys,” Mater. Letters, 60 (2006) 1654-1658.
28. J. Toscano, R. Vaßen, A. Gil, M. Subanovic, D. Naumenko, L. Singheiser and W. J. Quadakkers, “Parameters affecting TGO growth and adherence on MCrAlY-bond coats for TBC's,” Surf. Coat. Tech. 201 (2006) 3906-3910.
29. J. Toscano, D. Naumenko, A. Gil, L. Singheiser and W. J. Quadakkers, “Parameters affecting TGO growth rate and the lifetime of TBC systems with MCrAlY-bondcoats,” Materials and Corrosion 59 (2008) 501-507.
30. E. J. Opila, “Volatility of Common Protective Oxides in High-Temperature Water Vapor: Current Understanding and Unanswered Questions,” *Mater. Sci. Forum*, 461-464 (2004) 765-774.
31. E. J. Opila and D. L. Myers, “Alumina Volatility in Water Vapor at Elevated Temperatures,” J. Am. Ceram. Soc., 87 (2004) 1701-1705.

32. W. Nowak, "High Temperature Corrosion of Alloys and Coatings in Gas-Turbines Fired with Hydrogen-Rich Syngas Fuels, PhD thesis, RWTH Technical University Aachen, Germany, 2014.
33. A. Chyrkin, R. Pillai, H. Ackermann, H. Hattendorf, S. Richter, W. Nowak, D. Grüner and W. J. Quadakkers, "," Corrosion Science, 96 (2015) 32–41.
34. R. Pillai, A. Chyrkin, T. Galiullin, E. Wessel, D. Grüner and W.J. Quadakkers, "External α-$Al_2O_3$ scale on Ni-base alloy 602 CA – Part II: Microstructural evolution," Corrosion Science, in press.
35. G. C. Rybicki and J. L. Smialek, "Effect of the θ–α-$Al_2O_3$ Transformation on the Oxidation Behavior of β-NiAl+Zr," *Oxidation of Metals* **31**, 275-304 (1989).
36. F. S. Pettit, E. H. Randklev and E. J. Felten, "Formation of $NiAl_2O_4$ by Solid State Reaction," J. Amer. Cer. Soc., 49 (1966) 199-203.
37. M. H. Sullivan and D. R. Mumm, "Vapor-Phase-Mediated Phenomena Associated with High Temperature, High Water Content Oxidation of MCrAlX Bond Coats," Oxid. Met. 82 (2014) 1-20.
38. M. J. Lance, J. A. Haynes and B. A. Pint, "The Effects of Temperature and Substrate Curvature on TBC Lifetime and Residual Stress in Alumina Scales beneath APS TBCs," Surface and Coatings Technology, 308 (2016) 19-23.

## Figure Captions

**Figure 1.** Specimen mass change as a function of cumulative exposure time in 1-h cycles at 1100°C (a) in dry air comparing results from ORNL (dashed line) and FZJ (solid line) and (b) ORNL data in dry (closed symbols) and wet air (open symbols).

**Figure 2.** SEM BSE images of polished cross-sections of the ORNL specimens after 500, 1-h cycles at 1100°C in (a-d) dry air and (e-h) wet air, (a,e) non-ODS NiCoCrAlYHfSi and CoNiCrAlY with oxide dispersions of (b,f) $Al_2O_3$, (c,g) $Y_2O_3$ and (d,h) 1%$Y_2O_3$ + 1%$HfO_2$. The inset in (c) shows an area where the scale spalled.

**Figure 3.** (a) SEM BSE cross-section of the scale formed on non-ODS CoNiCrAlY after 500, 1-h cycles at 1100°C in dry air. The SEM EDS maps show the (b) Y, (c) O, (d) Al, (e) Cr and (f) Ni.

**Figure 4**. Microstructure measurements of specimens exposed to wet and dry air at 1100°C for 500 1-h cycles (a) scale thickness and (b) β-phase depletion beneath the scale. The whiskers show the minimum and maximum values measured and the boxes are the 25% and 75% values with the median value marked as the horizontal line in the box.

**Figure 5**. SEM BSE images in the substrate ~200 μm beneath the scale after 500, 1-h cycles in wet air, (a) non-ODS NiCoCrAlYHfSi and CoNiCrAlY with oxide dispersions of (b) $Al_2O_3$, (c) $Y_2O_3$ and (d) 1%$Y_2O_3$ + 1%$HfO_2$.

**Figure 6.** SEM EDS Cr elemental maps generated for specimens exposed for 500, 1-h cycles at 1100°C in (a-d) dry air and (e-h) wet air; (a,e) non-ODS NiCoCrAlYHfSi and

CoNiCrAlY with oxide dispersions of (b,f) $Al_2O_3$, (c,g) $Y_2O_3$ and (d,h) 1%$Y_2O_3$ + 1%$HfO_2$.

**Figure 7.** SEM BSE images in the center of the substrate after 500, 1-h cycles in wet air, (a) non-ODS NiCoCrAlYHfSi and (b) CoNiCrAlY with 1%$Y_2O_3$ + 1%$HfO_2$.

**Figure 8.** EBSD maps from the FZJ ODS CoNiCrAlY specimen with 1%$Y_2O_3$+1%$HfO_2$ oxidized for 500, 1-h cycles in dry air at 1100°C (a) near the interface of the β depletion zone and (b) ~200 µm below the surface.

**Figure 9**. Specimen mass gain during isothermal exposure at 1100°C in air with 10%$H_2O$. Noise in the system occurred during the exposure of the CoNiCrAlY specimen with 1%$Y_2O_3$ + 1%$HfO_2$.

**Figure 10.** SEM BSE polished cross section images after 100 h in wet air of (a) non-ODS NiCoCrAlYHfSi and CoNiCrAlY with oxide dispersions of (b) $Al_2O_3$, (c) $Y_2O_3$ and (d) 1%$Y_2O_3$ + 1%$HfO_2$.

**Figure 11.** STEM BF and HAADF cross-section images of the scale formed after 100 h isothermal oxidation in wet air on (a) non-ODS NiCoCrAlYHfSi and CoNiCrAlY with oxide dispersions of (b) $Al_2O_3$, (c) $Y_2O_3$ and (d) 1%$Y_2O_3$ + 1%$HfO_2$. All of the images are at the same magnification.

**Figure 12**. STEM HAADF cross-section images of the outer scale formed after 100 h isothermal oxidation in wet air on (a) non-ODS NiCoCrAlYHfSi and CoNiCrAlY with oxide dispersions of (b) $Al_2O_3$, (c) $Y_2O_3$ and (d) 1%$Y_2O_3$ + 1%$HfO_2$. All of the images are at the same magnification.

**Figure 13.** (a) STEM BF cross-section image of the scale formed after 100 h isothermal oxidation in wet air on non-ODS NiCoCrAlYHfSi. Both the (b) outer and (c) inner layers were identified as α-$Al_2O_3$ using the electron diffraction patterns along the $[2\bar{1}\bar{1}0]$ zone axis.

**Figure 14.** STEM HAADF cross-section images and associated EDS maps of the scales formed after 100 h isothermal oxidation in wet air on (a) non-ODS NiCoCrAlYHfSi and CoNiCrAlY with oxide dispersions of (b) $Al_2O_3$, (c) $Y_2O_3$ and (d) 1%$Y_2O_3$ + 1%$HfO_2$.

**Figure 15.** (a) STEM BF cross-section of the scale formed on $Al_2O_3$-dispersed CoNiCrAlY after 100h isothermal exposure at 1100°C in wet air. The STEM EDS maps show the (b) O, (c) Al, (d) Y and (e) Cr.

**Figure 16.** STEM TKD of the scale cross-sections formed after 100h isothermal exposure at 1100°C in wet air on CoNiCrAlY with dispersions of (a) $Al_2O_3$, (b) $Y_2O_3$ and (c) 1%$Y_2O_3$ + 1%$HfO_2$.

Table 1. Chemical composition (wt.%) of free-standing coatings after 6 h of ball milling determined by inductively coupled plasma optical emission spectroscopy: values for O, C, and N determined by combustion analysis are given in ppmw

| Material | Co | Ni | Cr | Al | Y | Hf | Si | Fe | Ti | O | C | N |
|---|---|---|---|---|---|---|---|---|---|---|---|---|
| No Addition (Amdry 9954) | 39.0† | 32.0† | 20.0† | 8.0† | 0.5† | <0.01# | <0.1# | <0.1# | <0.01# | <500# | <100# | <100# |
| *No Addition(High Hf) (Amdry 386) | 22.0 | 47.1 | 16.3 | 12.5 | 0.68 | 0.27 | 0.32 | 0.05 | 0.009 | <500# | 17 | 32 |
| 2%$Al_2O_3$ | 38.4 | 32.3 | 20.0 | 8.9 | 0.35 | <0.03 | 0.026 | 0.40 | 0.001 | 9650 | 3140 | 54 |
| 2% $Y_2O_3$ | 38.7 | 32.4 | 20.0 | 8.1 | **1.78** | <0.02 | 0.021 | 0.27 | 0.001 | 5080 | 2380 | 33 |
| 1%$Y_2O_3$+$HfO_2$ | 38.5 | 32.2 | 19.9 | 8.0 | **1.19** | **0.70** | 0.014 | 0.24 | 0.002 | 4800 | 2410 | 43 |

† - nominal values; # - values typically measured in Amdry 9954 coatings sprayed with same LPPS-process

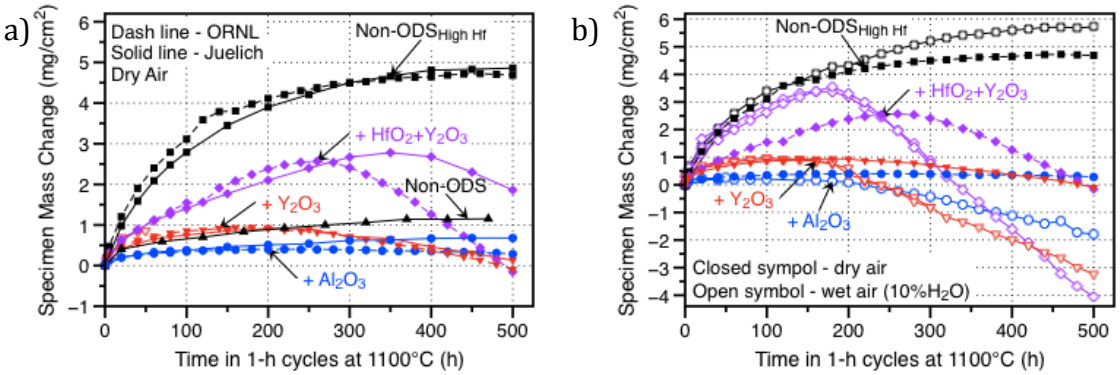


**Figure 1.** Specimen mass change as a function of cumulative exposure time in 1-h cycles at 1100°C (a) in dry air comparing results from ORNL (dashed line) and FZJ (solid line) and (b) ORNL data in dry (closed symbols) and wet air (open symbols).

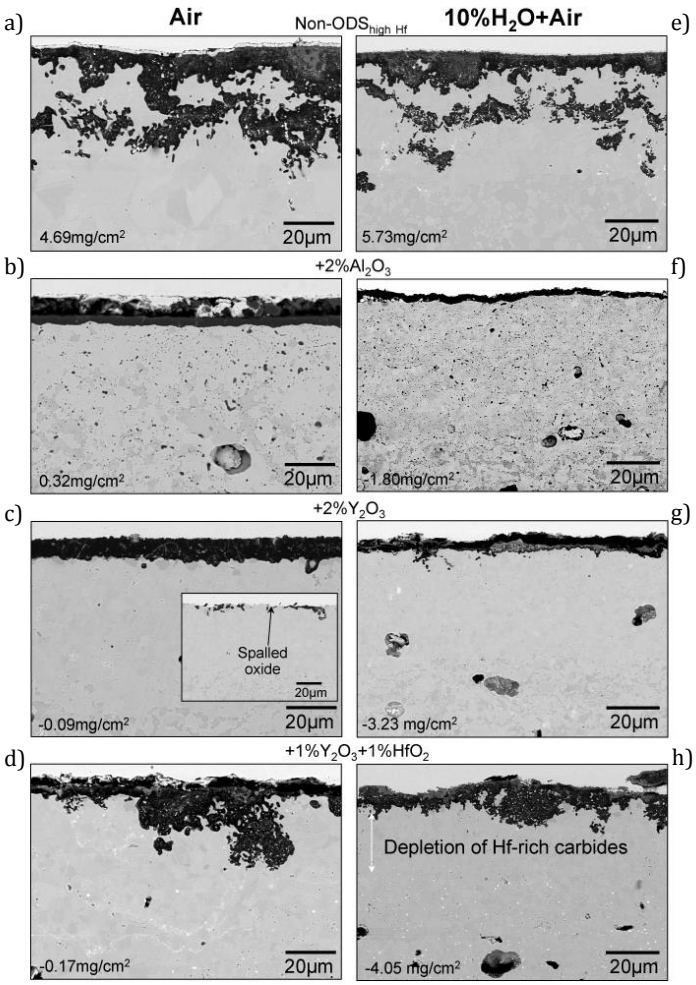


**Figure 2.** SEM BSE images of polished cross-sections of the ORNL specimens after 500, 1-h cycles at 1100°C in (a-d) dry air and (e-h) wet air, (a,e) non-ODS NiCoCrAlYHfSi and CoNiCrAlY with oxide dispersions of (b,f) $Al_2O_3$, (c,g) $Y_2O_3$ and (d,h) 1%$Y_2O_3$ + 1%$HfO_2$. The inset in (c) shows an area where the scale spalled.

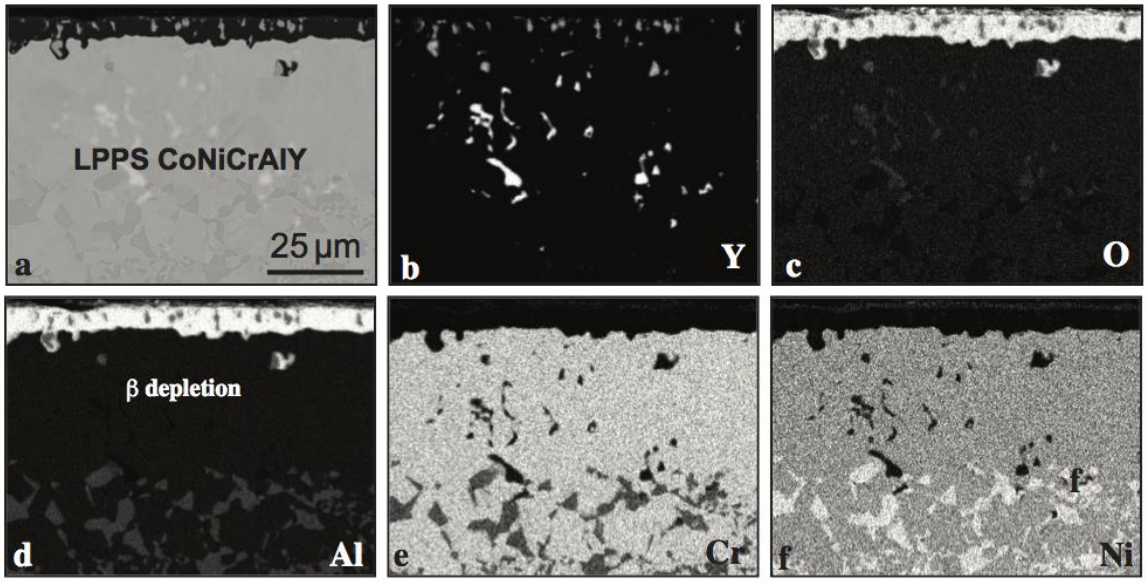


**Figure 3.** (a) SEM BSE cross-section of the scale formed on non-ODS CoNiCrAlY after 500, 1-h cycles at 1100°C in dry air. The SEM EDS maps show the (b) Y, (c) O, (d) Al, (e) Cr and (f) Ni.

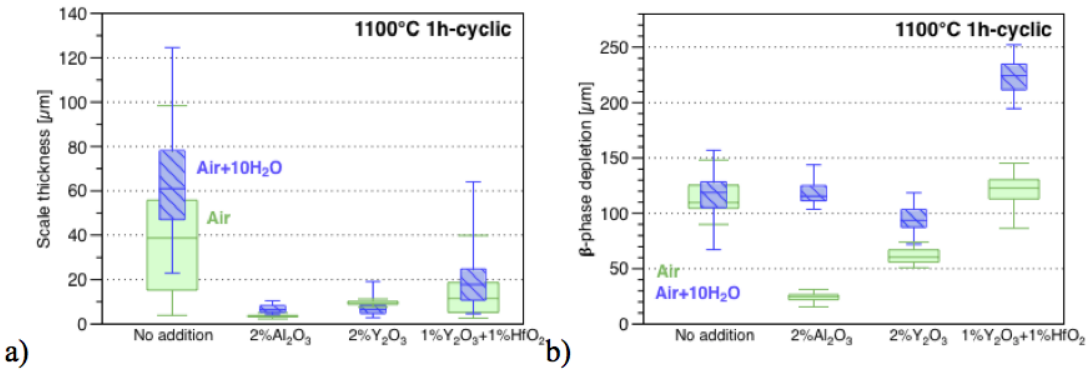


**Figure 4**. Microstructure measurements of specimens exposed to wet and dry air at 1100°C for 500 1-h cycles (a) scale thickness and (b) β-phase depletion beneath the scale. The whiskers show the minimum and maximum values measured and the boxes are the 25% and 75% values with the median value marked as the horizontal line in the box.

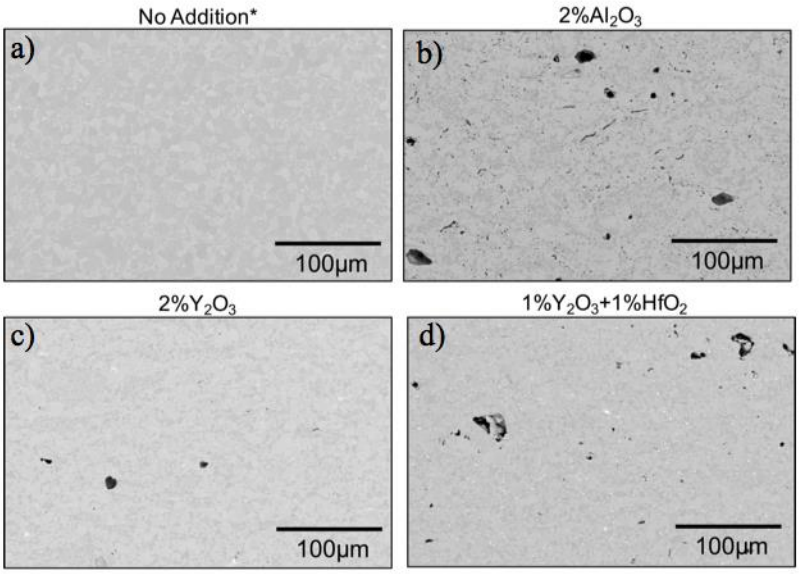


**Figure 5**. SEM BSE images in the substrate ~200 µm beneath the scale after 500, 1-h cycles in wet air, (a) non-ODS NiCoCrAlYHfSi and CoNiCrAlY with oxide dispersions of (b) $Al_2O_3$, (c) $Y_2O_3$ and (d) 1%$Y_2O_3$ + 1%$HfO_2$.

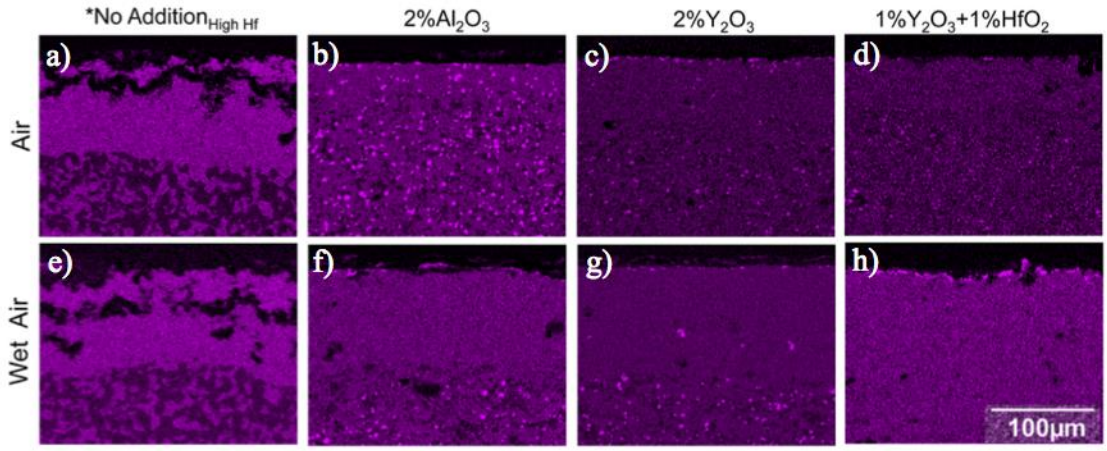


**Figure 6.** SEM EDS Cr elemental maps generated for specimens exposed for 500, 1-h cycles at 1100°C in (a-d) dry air and (e-h) wet air; (a,e) non-ODS NiCoCrAlYHfSi and CoNiCrAlY with oxide dispersions of (b,f) $Al_2O_3$, (c,g) $Y_2O_3$ and (d,h) 1%$Y_2O_3$ + 1%$HfO_2$.

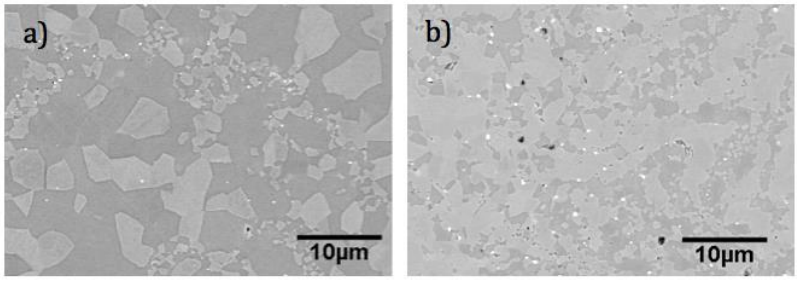


**Figure 7.** SEM BSE images in the center of the substrate after 500, 1-h cycles in wet air, (a) non-ODS NiCoCrAlYHfSi and (b) CoNiCrAlY with 1%$Y_2O_3$ + 1%$HfO_2$.

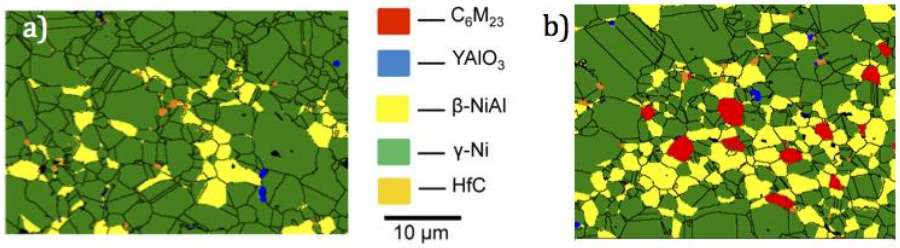


**Figure 8.** EBSD maps from the FZJ ODS CoNiCrAlY specimen with 1%$Y_2O_3$+1%$HfO_2$ oxidized for 500, 1-h cycles in dry air at 1100°C (a) near the interface of the β depletion zone and (b) ~200 μm below the surface.

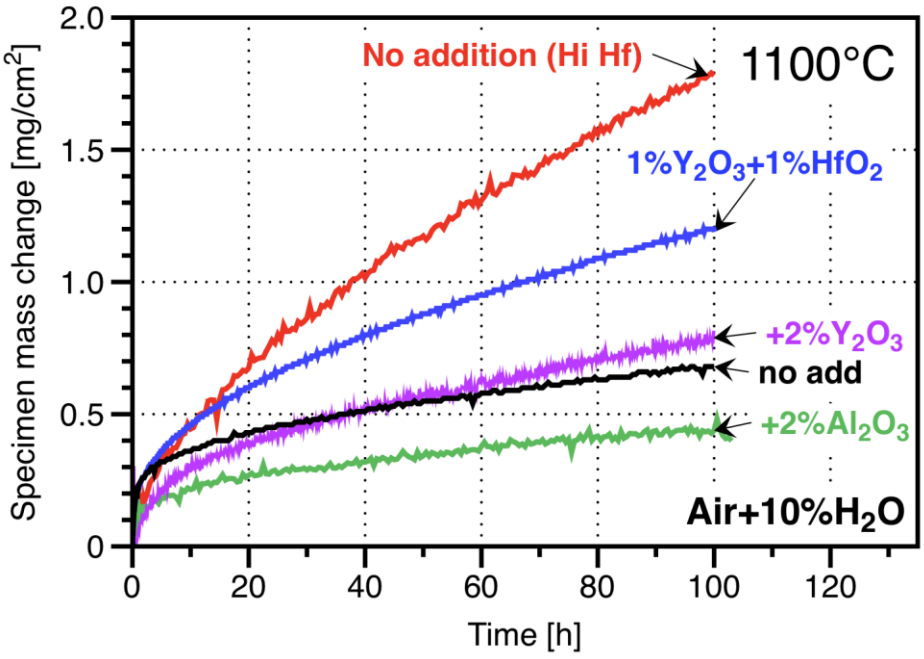


**Figure 9**. Specimen mass gain during isothermal exposure at 1100°C in air with 10%$H_2O$. Noise in the system occurred during the exposure of the CoNiCrAlY specimen with 1%$Y_2O_3$ + 1%$HfO_2$.

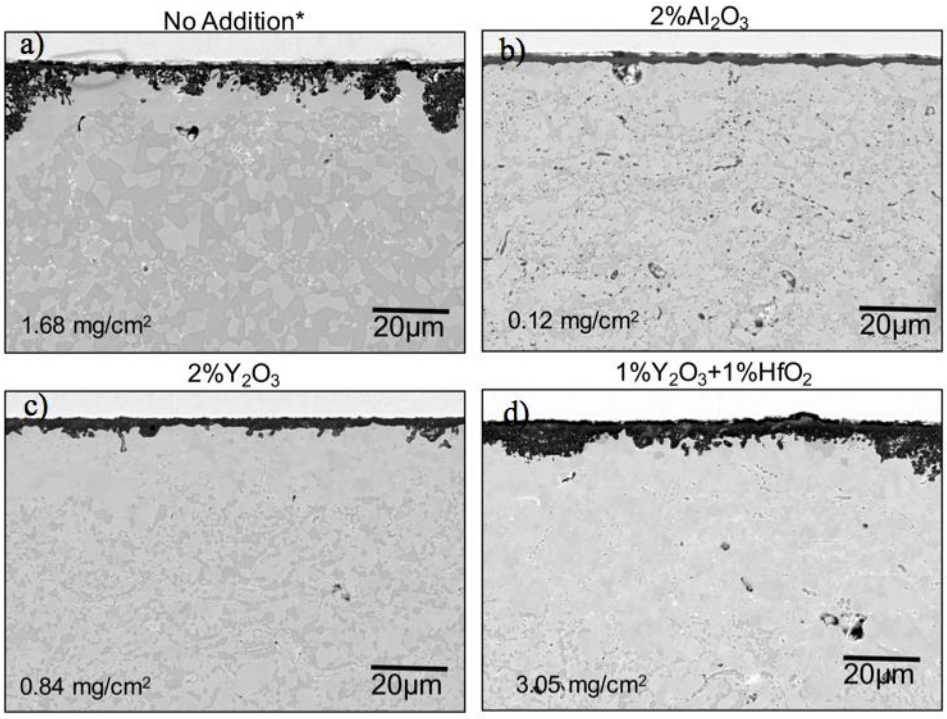


**Figure 10.** SEM BSE polished cross section images after 100 h in wet air of (a) non-ODS NiCoCrAlYHfSi and CoNiCrAlY with oxide dispersions of (b) $Al_2O_3$, (c) $Y_2O_3$ and (d) 1%$Y_2O_3$ + 1%$HfO_2$.

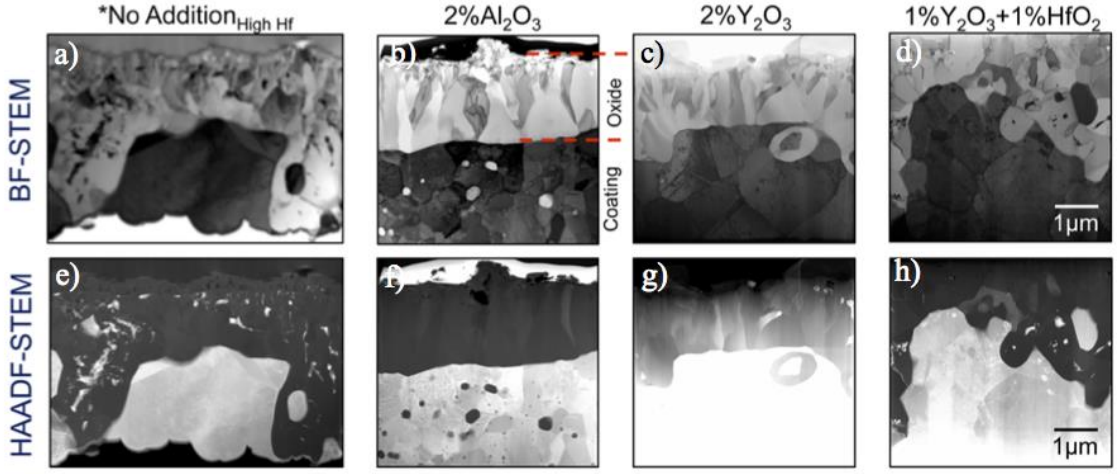


**Figure 11.** STEM BF and HAADF cross-section images of the scale formed after 100 h isothermal oxidation in wet air on (a) non-ODS NiCoCrAlYHfSi and CoNiCrAlY with oxide dispersions of (b) $Al_2O_3$, (c) $Y_2O_3$ and (d) 1%$Y_2O_3$ + 1%$HfO_2$. All of the images are at the same magnification.

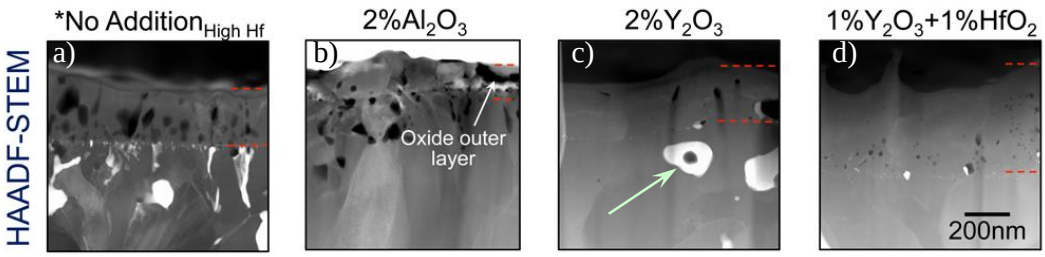


**Figure 12**. HAADF-STEM images of the outer scale cross-section formed after 100 h in wet air on (a) non-ODS CoNiCrAlYHfSi and CoNiCrAlY with oxide dispersions of (b) $Al_2O_3$, (c) $Y_2O_3$ and (d) 1%$Y_2O_3$ + 1%$HfO_2$. All of the images are at the same magnification.

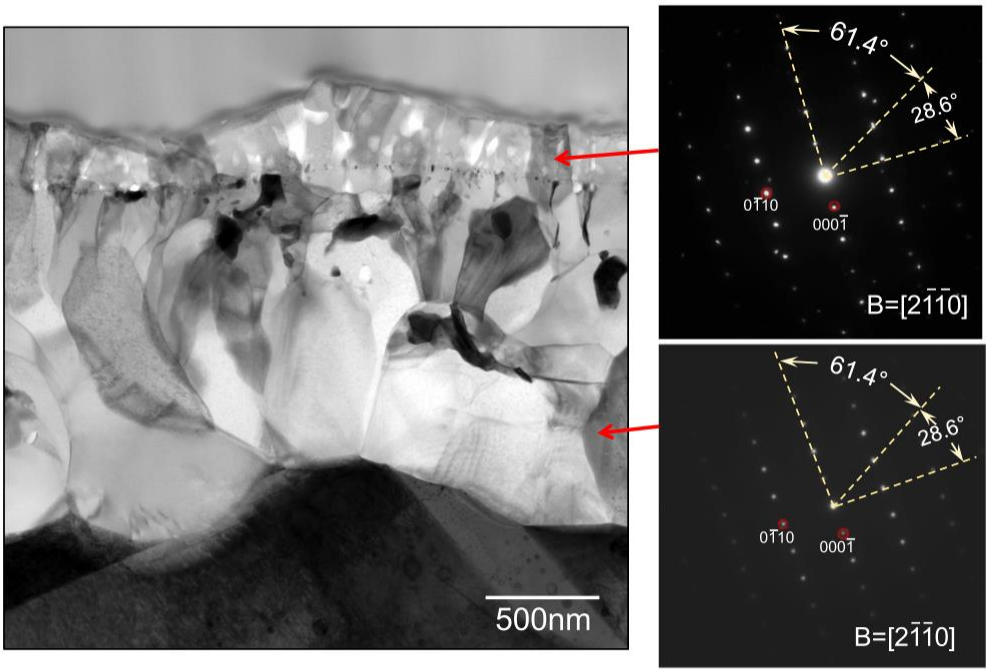


**Figure 13.** (a) STEM BF cross-section image of the scale formed after 100 h isothermal oxidation in wet air on non-ODS NiCoCrAlYHfSi. Both the (b) outer and (c) inner layers were identified as α-$Al_2O_3$ using the electron diffraction patterns along the [2$\bar{1}\bar{1}$0] zone axis.

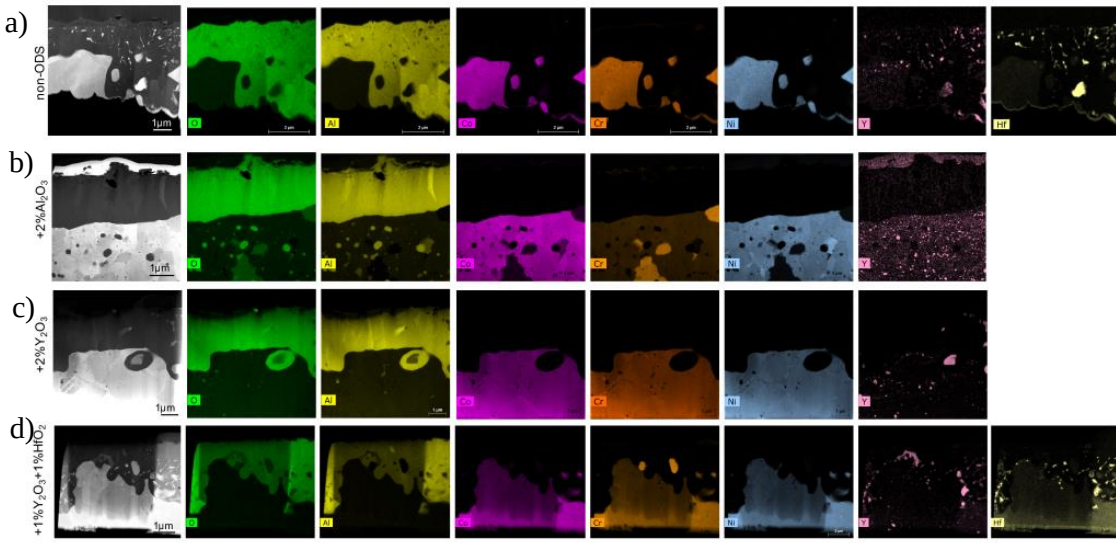


**Figure 14.** HAADF-STEM images of the scale cross-section and associated EDS maps of the scales formed after 100 h in wet air on (a) non-ODS NiCoCrAlYHfSi and CoNiCrAlY with oxide dispersions of (b) $Al_2O_3$, (c) $Y_2O_3$ and (d) 1%$Y_2O_3$ + 1%$HfO_2$.

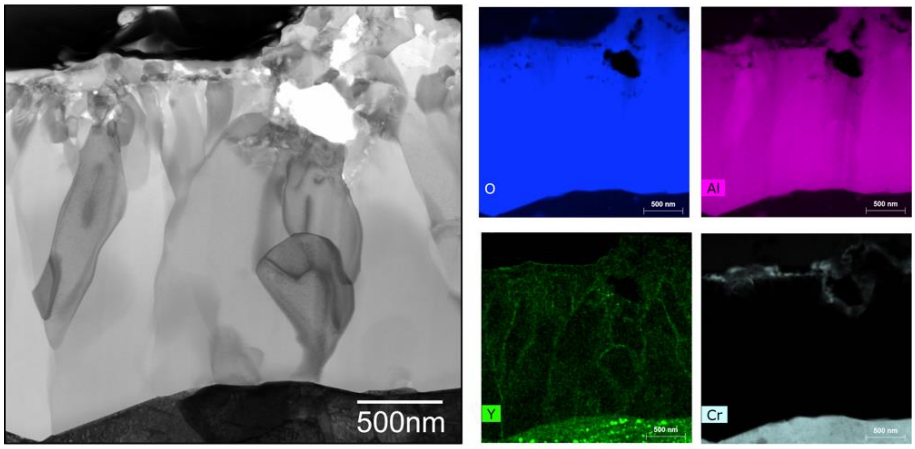


**Figure 15.** (a) STEM BF cross-section of the scale formed on $Al_2O_3$-dispersed CoNiCrAlY after 100h isothermal exposure at 1100°C in wet air. The STEM EDS maps show the (b) O, (c) Al, (d) Y and (e) Cr.

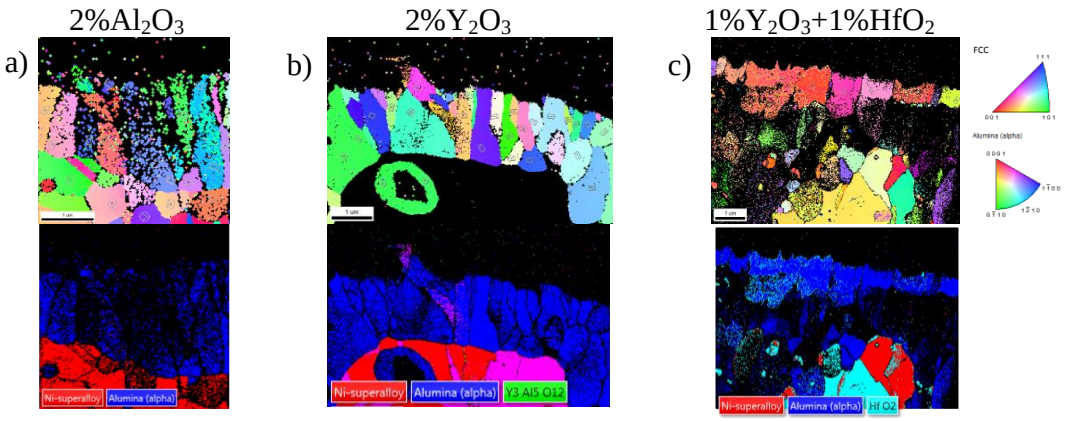


**Figure 16.** STEM TKD of the scale cross-sections formed after 100h isothermal exposure at 1100°C in wet air on CoNiCrAlY with dispersions of (a) $Al_2O_3$, (b) $Y_2O_3$ and (c) $1\%Y_2O_3 + 1\%HfO_2$.

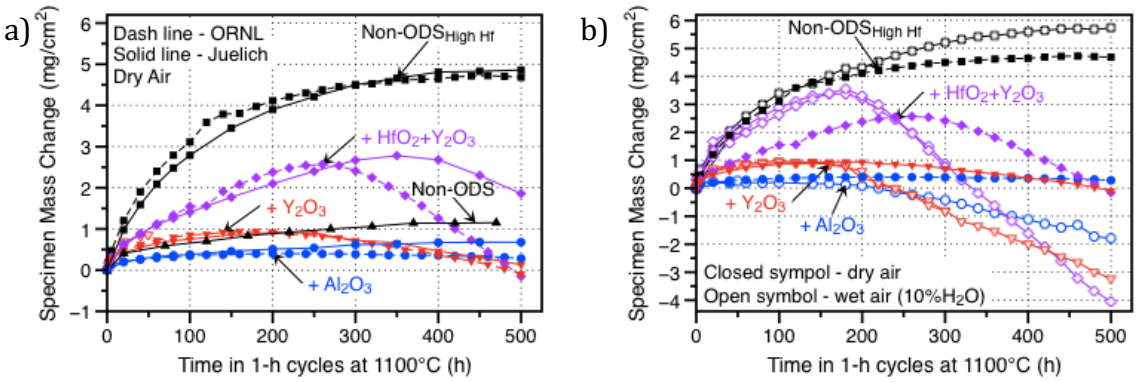


**Figure 1.** Specimen mass change as a function of cumulative exposure time in 1-h cycles at 1100°C (a) in dry air comparing results from ORNL (dashed line) and FZJ (solid line) and (b) ORNL data in dry (closed symbols) and wet air (open symbols).

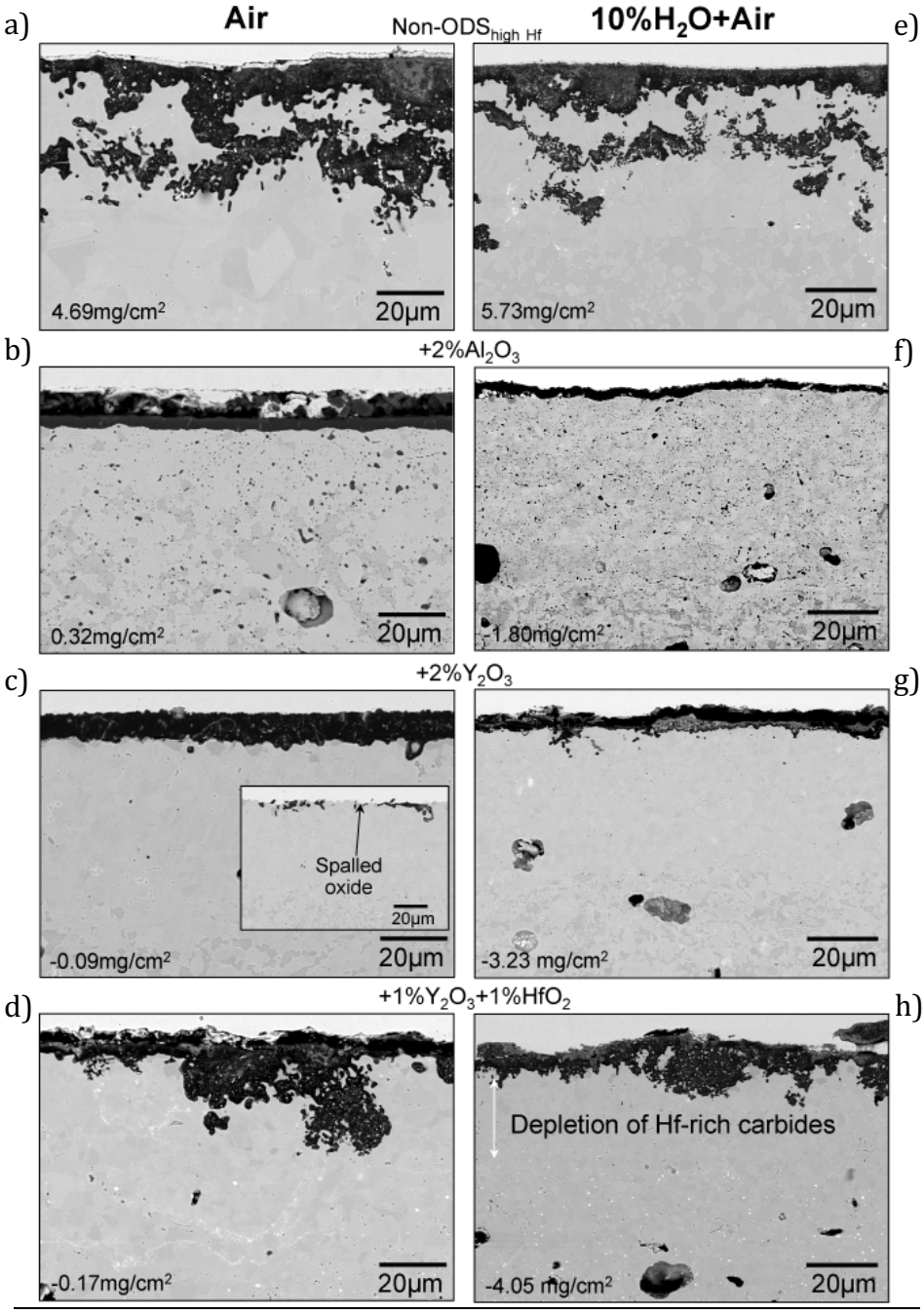


**Figure 2.** SEM BSE images of polished cross-sections of the ORNL specimens after 500, 1-h cycles at 1100°C in (a-d) dry air and (e-h) wet air, (a,e) non-ODS NiCoCrAlYHfSi and CoNiCrAlY with oxide dispersions of (b,f) $Al_2O_3$, (c,g) $Y_2O_3$ and (d,h) 1%$Y_2O_3$ + 1%$HfO_2$. The inset in (c) shows an area where the scale spalled.

Fig3

Click here to download Non-colour figure 3 JMCAN+ SEM FZJ.png

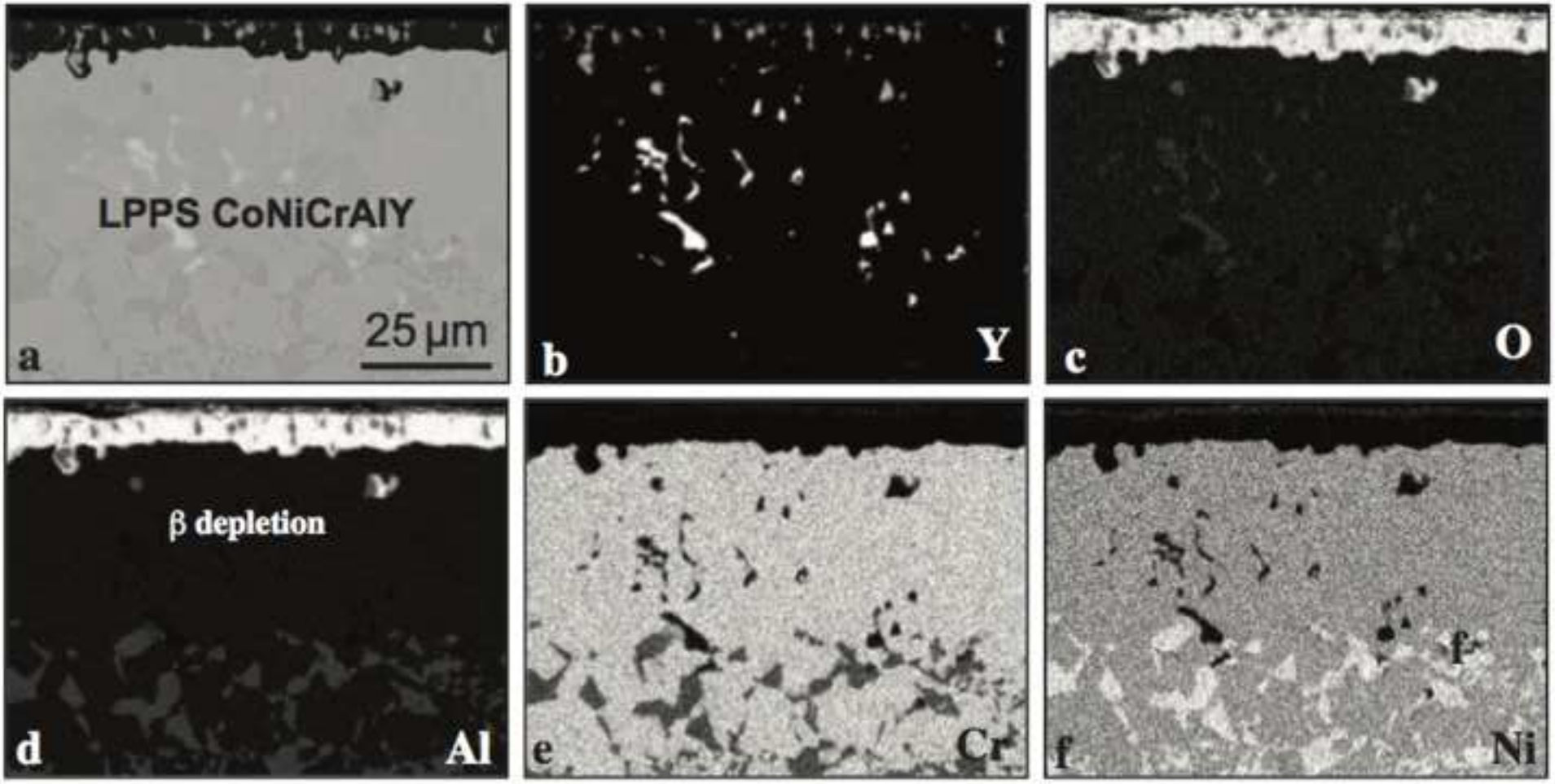

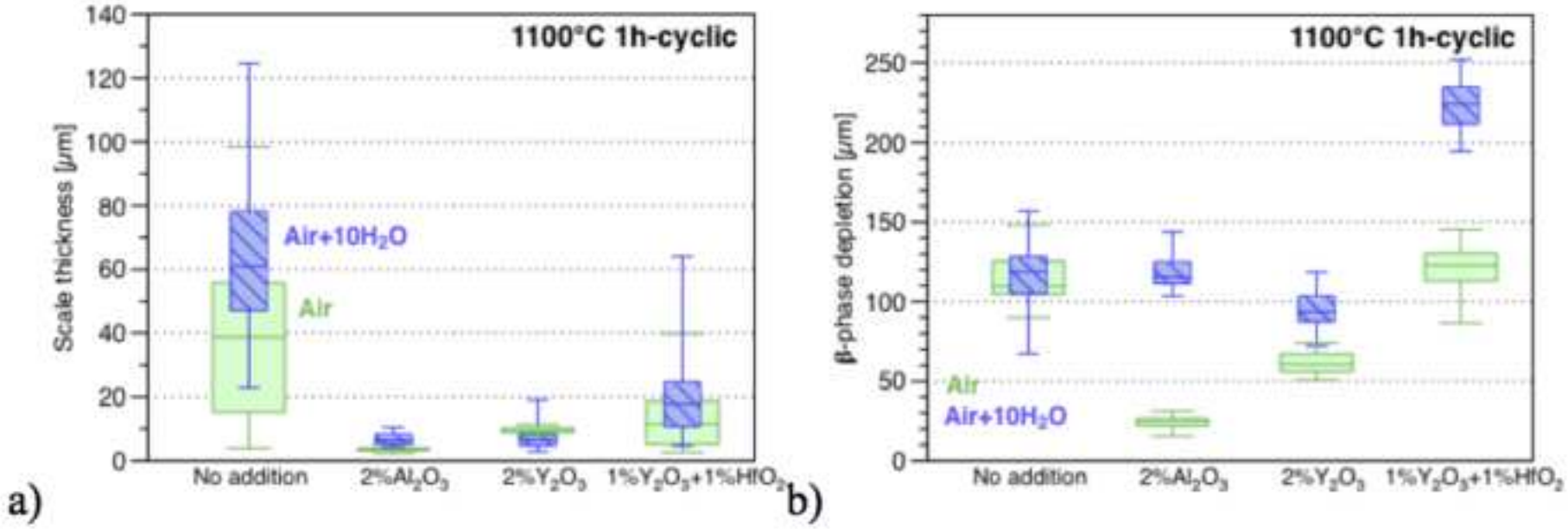


**Figure 4**. Microstructure measurements of specimens exposed to wet and dry air at 1100°C for 500 1-h cycles (a) scale thickness and (b) β-phase depletion beneath the scale. The whiskers show the minimum and maximum values measured and the boxes are the 25% and 75% values with the median value marked as the horizontal line in the box.

Fig5

Click here to download Non-colour figure 5 SEM.png

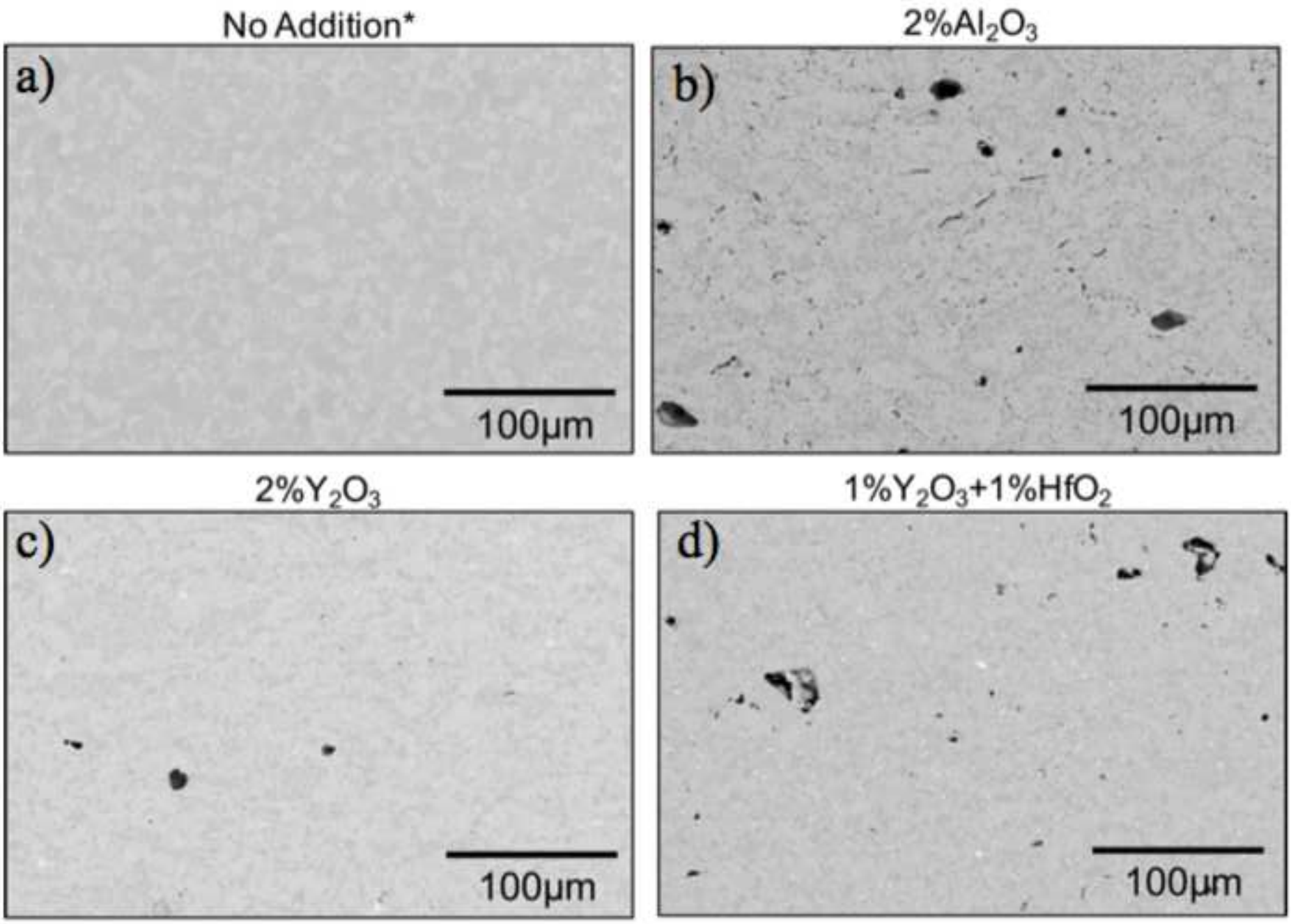

Fig6

Click here to download Colour figure (print) 6 SEM.png

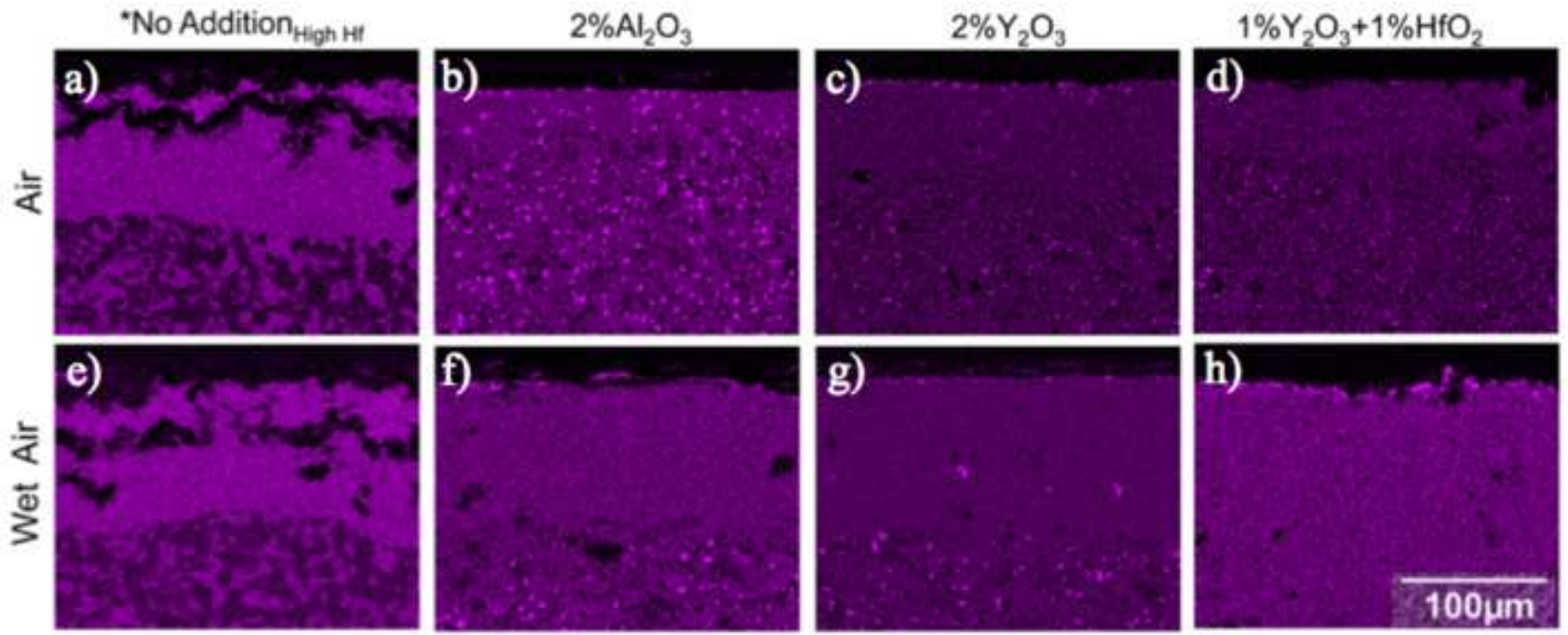

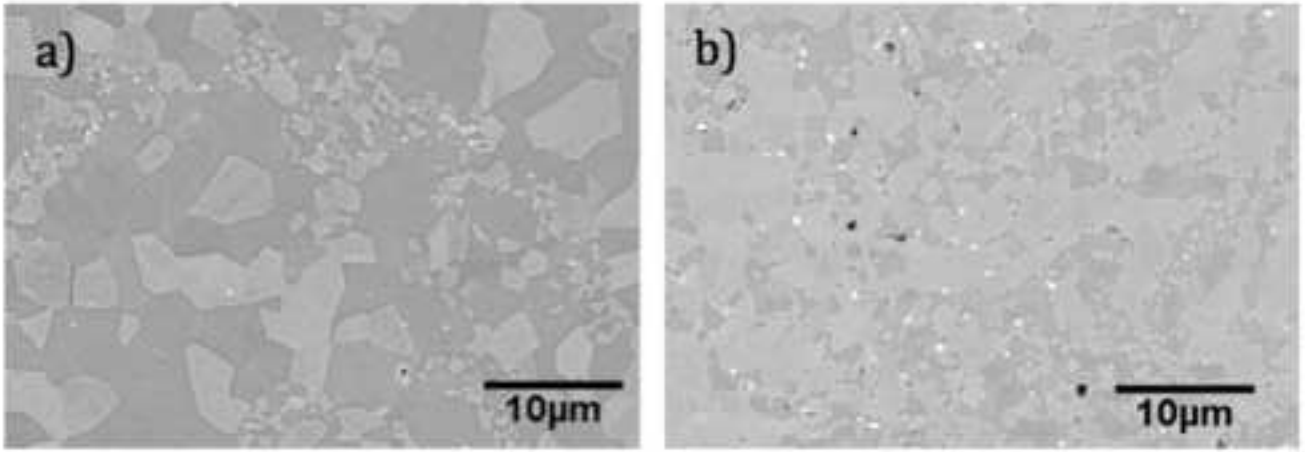


**Figure 7.** SEM BSE images in the center of the substrate after 500, 1-h cycles in wet air, (a) non-ODS NiCoCrAlYHfSi and (b) CoNiCrAlY with 1%$Y_2O_3$ + 1%$HfO_2$.

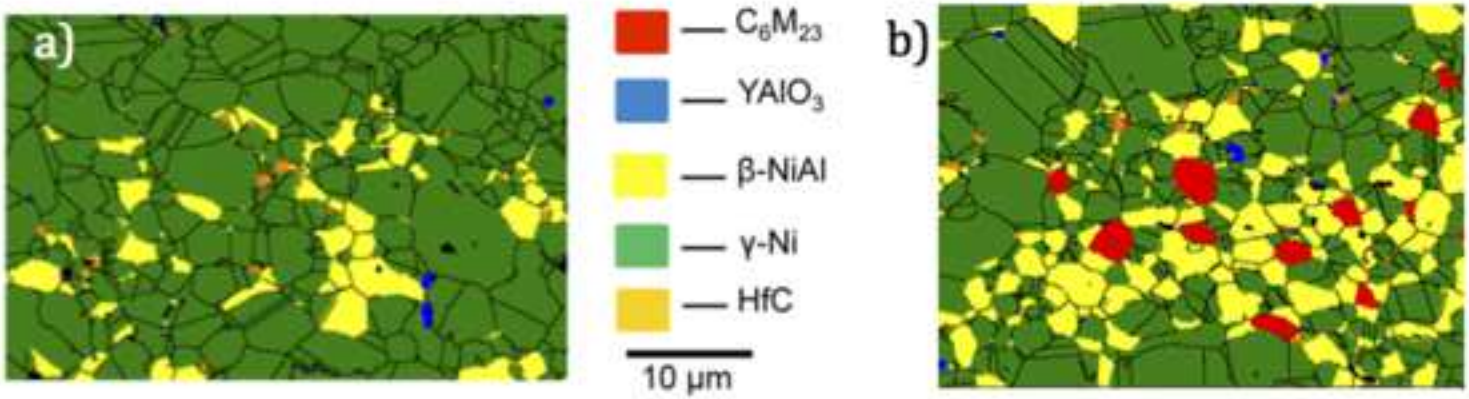


**Figure 8.** EBSD maps from the FZJ ODS CoNiCrAlY specimen with 1%$Y_2O_3$+1%$HfO_2$ oxidized for 500, 1-h cycles in dry air at 1100°C (a) near the interface of the β depletion zone and (b) ~200 µm below the surface.

Fig 9

Click here to download Colour figure (print) 9. 1100C TGA+.tiff

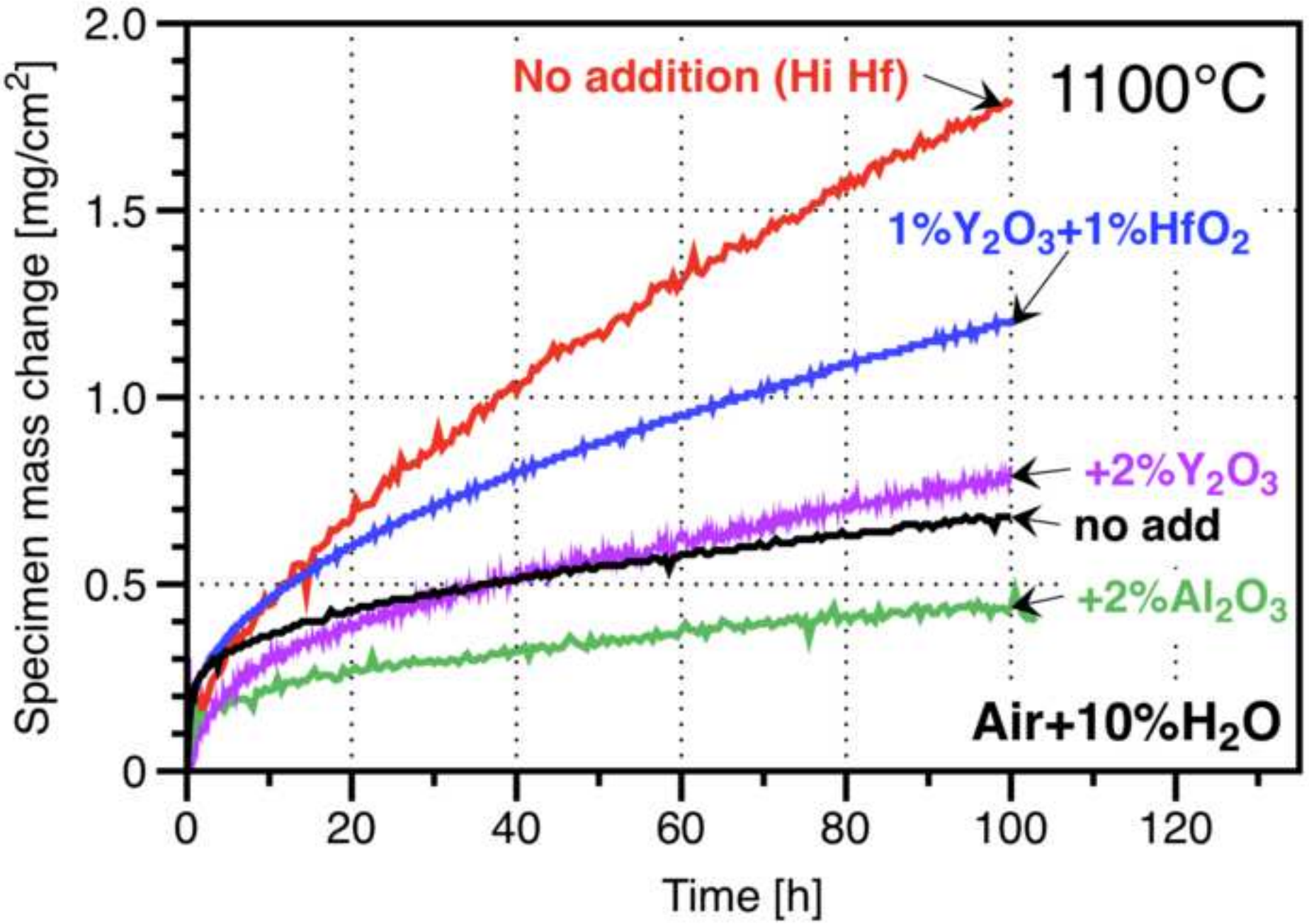

Fig 10

Click here to download Non-colour figure 10. SEM.png

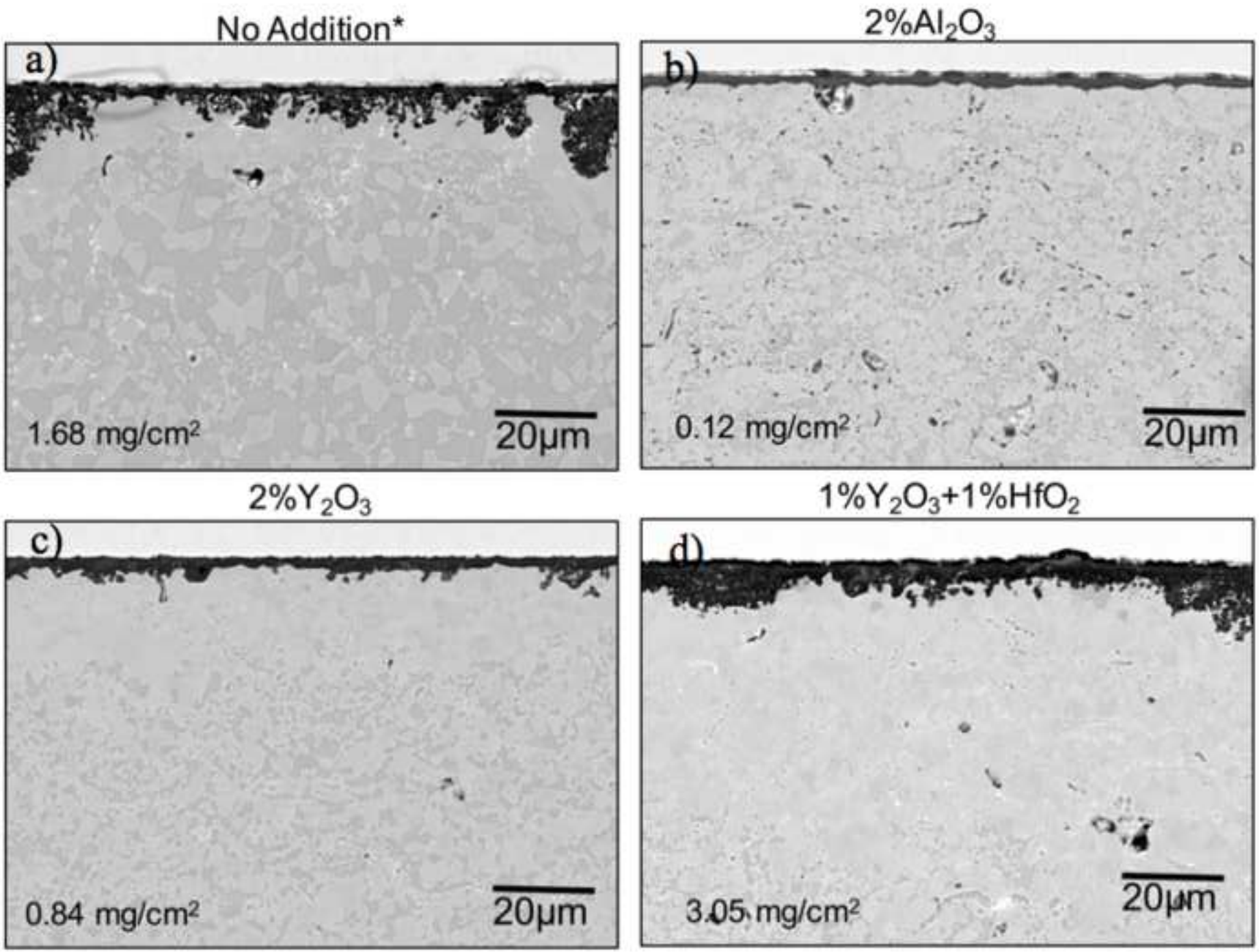

Fig 11

Click here to download Colour figure (print) 11 TEM.png

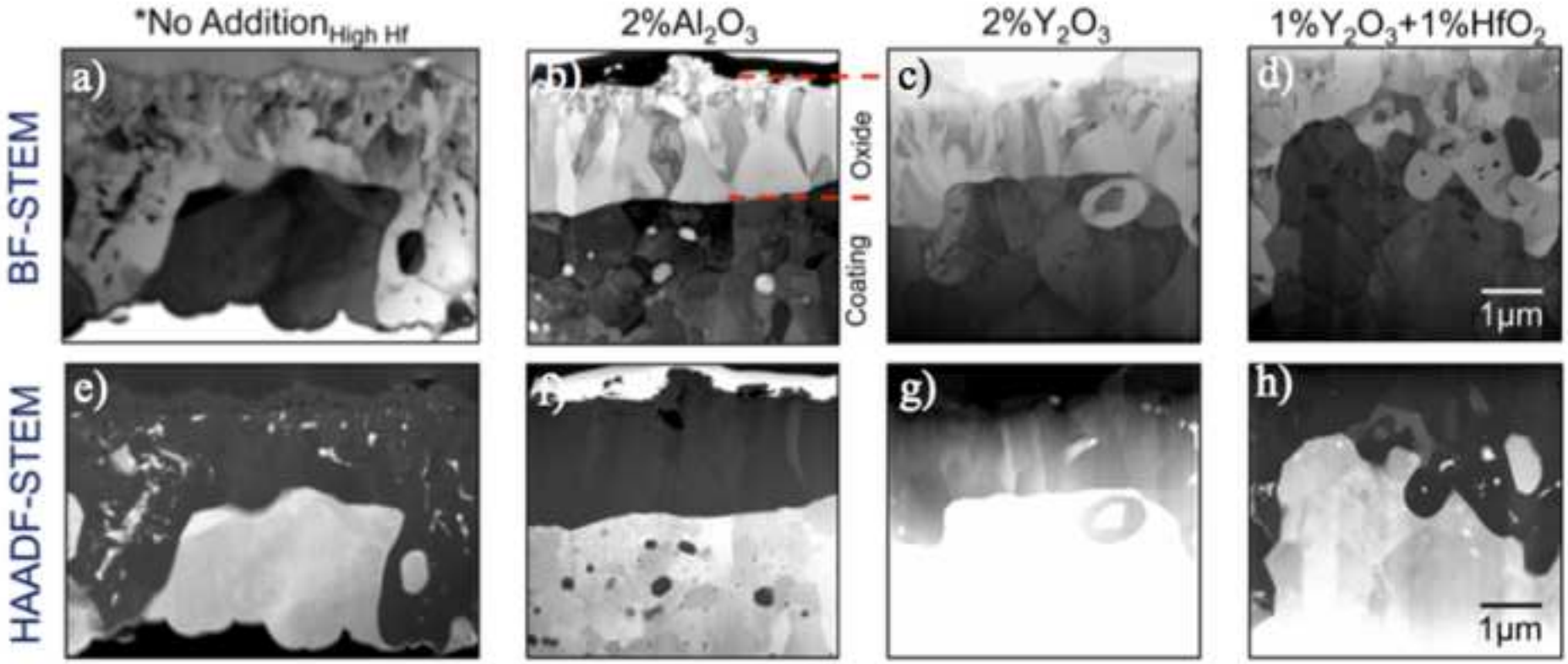

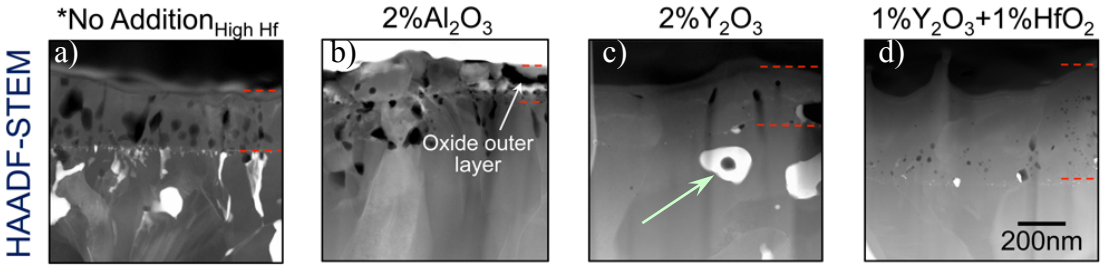


**Figure 12**. HAADF-STEM images of the outer scale cross-section formed after 100 h in wet air on (a) non-ODS CoNiCrAlYHfSi and CoNiCrAlY with oxide dispersions of (b) $Al_2O_3$, (c) $Y_2O_3$ and (d) $1\%Y_2O_3 + 1\%HfO_2$. All of the images are at the same magnification.

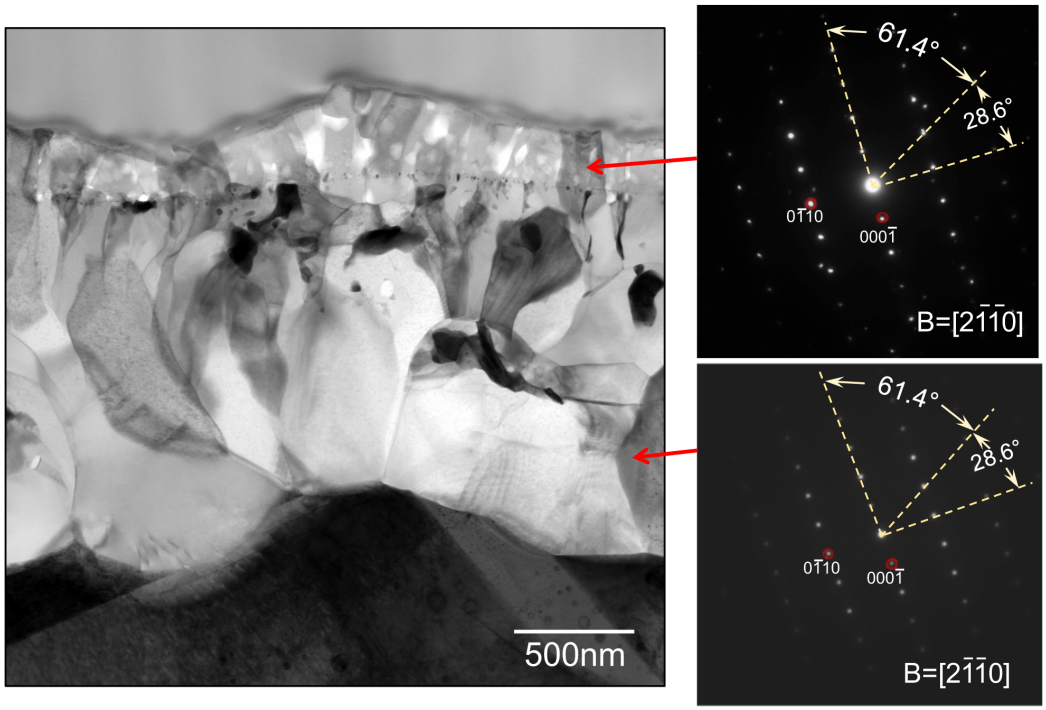


**Figure 13.** (a) BF-STEM image of the scale cross-section formed after 100 h in wet air on non-ODS CoNiCrAlYHfSi. Both the (b) outer and (c) inner layers were identified as $\alpha$-$Al_2O_3$ using the electron diffraction patterns along the [2$\bar{1}\bar{1}$0] zone axis.

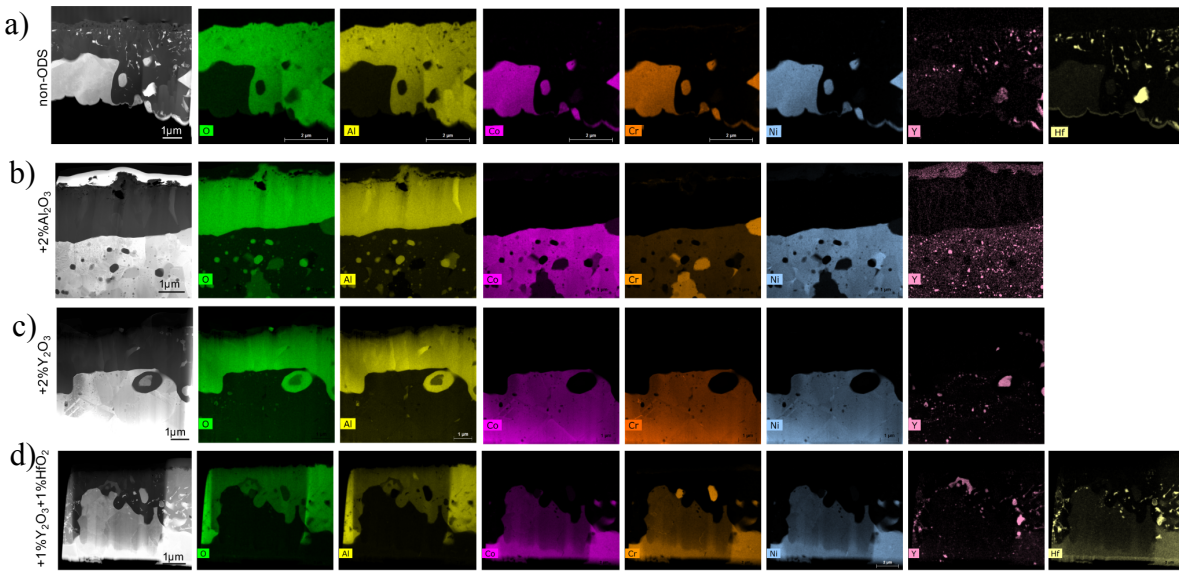


**Figure 14.** HAADF-STEM images of the scale cross-section and associated EDS maps of the scales formed after 100 h in wet air on (a) non-ODS NiCoCrAlYHfSi and CoNiCrAlY with oxide dispersions of (b) $Al_2O_3$, (c) $Y_2O_3$ and (d) 1%$Y_2O_3$ + 1%$HfO_2$.

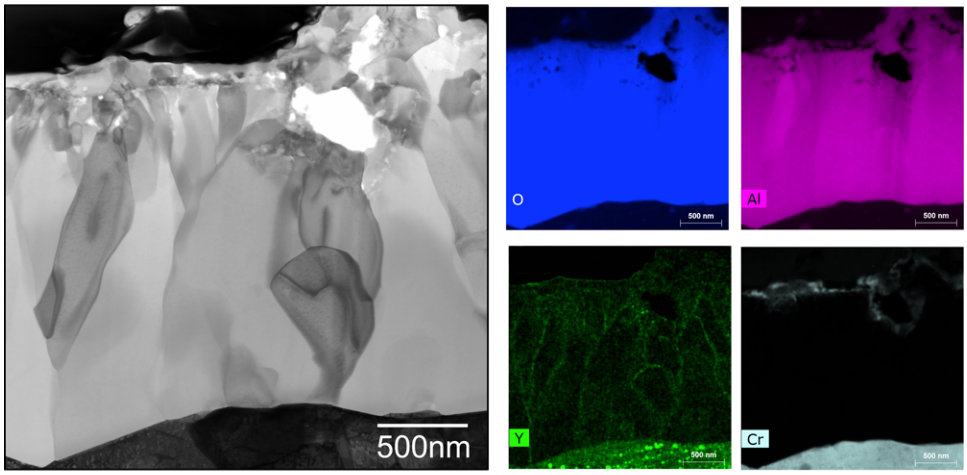


**Figure 15.** (a) BF-STEM cross-section of the scale formed on $Al_2O_3$-dispersed CoNiCrAlY after 100h isothermal exposure at 1100°C in wet air. The STEM EDS maps show the (b) O, (c) Al, (d) Y and (e) Cr.

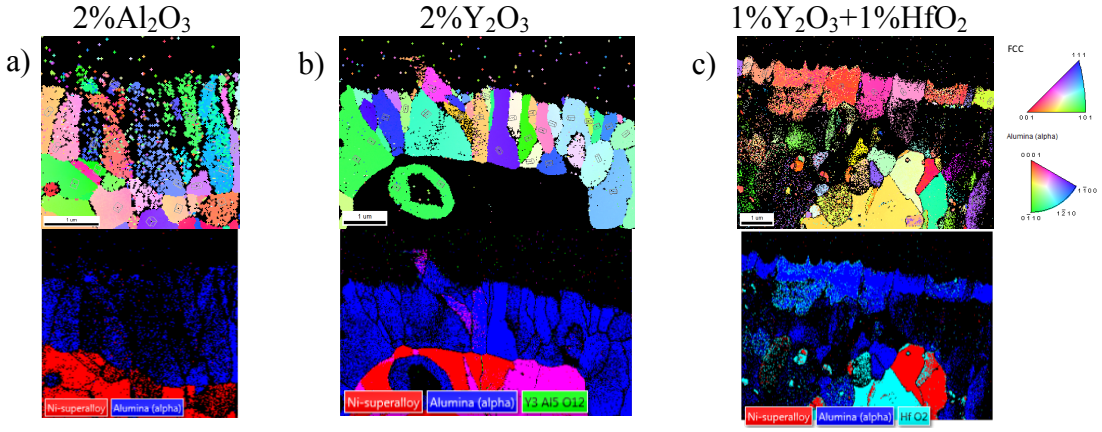


**Figure 16.** TKD and phase maps of the scale cross-sections formed after 100h isothermal exposure at 1100°C in wet air on CoNiCrAlY with dispersions of (a) $Al_2O_3$, (b) $Y_2O_3$ and (c) $1\%Y_2O_3 + 1\%HfO_2$.